Physical mechanisms and parameters for models of microstructure evolution under irradiation in Fe alloys – Part I: Pure Fe

L. Malerba [a,*], N. Anento [b], J.P. Balbuena [c], C.S. Becquart [d], N. Castin [e], M.J. Caturla [c], C. Domain [f], C. Guerrero [a], C.J. Ortiz [g], B. Pannier [d,f], A. Serra [b]

[a] *Energy Materials Division, Department of Technology, Centre for Research on Energy, Environment and Technology (CIEMAT), Avda. Complutense 40, 28040 Madrid, Spain*
[b] *Department of Civil and Environmental Engineering, Universitat Politècnica de Catalunya, Jordi Girona, 1-3, 08034 Barcelona, Spain*
[c] *Department of Applied Physics, University of Alicante, E-03690 Alicante, Spain*
[d] *Unité Matériaux et Transformations (UMET), UMR 8207 CNRS, Univ. Lille, INRAE, Centrale Lille, F-59000 Lille, France*
[e] *Institute of Nuclear Materials Science, Belgian Nuclear Research Centre (SCK-CEN), Boeretang 200, 2400 Mol, Belgium*
[f] *Département Matériaux et Mécanique des Composants, EDF R&D, Les Renardières, F-77250 Moret Sur Loing, France*
[g] *National Fusion Laboratory, Centre for Research on Energy, Environment and Technology (CIEMAT), Avda. Complutense 40, 28040 Madrid, Spain*

ARTICLE INFO

ABSTRACT

This paper is the first of three that overview the main mechanisms that drive the microstructure evolution in Fe alloys under irradiation. It focuses on pure α-Fe and compiles the parameters that describe quantitatively the mobility and stability of point-defects and especially their clusters, including possible reactions and criteria to decide when they should react. These parameters are the result of several years of calculations and application in microstructure evolution models. They are mainly collected from the literature and the parameter choice tries to reconcile different sets of values that, while being in general qualitatively similar, are often quantitatively not coincident. A few calculation results are presented here for the first time to support specific approximations concerning defect properties or features. Since calculations cannot cover all possible defect configurations, the definition of these parameters often requires educated guesses to fill knowledge gaps. These guesses are here listed and discussed whenever relevant. This is therefore a "hands-on" paper that: (i) collects in a single report most microstructure evolution parameters that are found in the literature for irradiated α-Fe, including a discussion of the most important mechanisms at play based on current knowledge; (ii) selects a ready-to-use set that can be employed in microstructure evolution models, such as those based on object kinetic Monte Carlo (OKMC) methods. This work also identifies parameters that are needed, but not known, hopefully prompting corresponding calculations in the future.

Introduction

Object kinetic Monte Carlo (OKMC) models have been used since the late 1990s to simulate the microstructure evolution in α-Fe [1–14] and its alloys [6,15–23] when subjected to irradiation with either ions or neutrons.

This simulation method requires that all the possible reactions between defects that drive the evolution of the microstructure be defined *a priori*. Parameters for these reactions are generally impossible to measure experimentally and should be obtained preferably from accurate calculation methods such as density functional theory (DFT), or empirical interatomic potentials (EIP), if DFT data are not available or accessible. Advanced microstructure evolution simulation methods that allow the on-the-fly calculation of the transition barriers, such as SEAKMC [24–26] or k-ART [27], which make systematic use of the activation-relaxation technique (ART) method [28] for saddle point search, do exist. These models do not require a predefined list of mechanisms and parameters to be compiled. However, they are affected by two serious limitations: firstly, the computational time is significantly increased and calculations that can be directly compared to the result of

---

microstructural examination in irradiation experiments cannot be performed with this approach; secondly, in most cases they still rely on EIPs, with the limitations that this imposes, especially when considering concentrated alloys, or alloys that contain several solutes [29]. It is in principle possible to apply these models using DFT calculations instead of EIPs [28], but then the required computing time becomes so long , that the possibility of using them to trace the evolution of the microstructure under irradiation conditions comparable with experiments is totally lost. Therefore, in order to simulate the behaviour of materials that are representative of real alloys, under irradiation conditions that are comparable with the experimental ones, the predefinition of the physical mechanisms and the relevant parameters to be implemented in the model remains a necessary, and difficult, task. In some cases, however, on-the-fly calculations can be used to determine some of the predefined physical mechanisms and relevant parameters that can be used in models such as OKMC, for example the diffusion coefficient of clusters of point-defects or their dissociation frequency can be calculated using on-the-fly methods, provided that the computing time to do so remains affordable.

OKMC models have been evolving over the years, by spanning increasingly larger timescales, and thus dose intervals, as well as including more details about the defect configurations [1–23]. Initially, only vacancies and self-interstitials, single and in clusters, were tracked, without making any distinction about their inherent characteristics. As more information arose from atomistic calculations, the models became more complex and different configurations of defects were distinguished and considered, so long as possible. This paper collects most of the state of the art of the information that is currently available on this subject. Importantly, some of the mechanisms and especially parameters presented in this work are of use also for cluster dynamics (or rate theory) models [30,31].

The fundamental physical processes that determine the evolution of the microstructure under irradiation can be reduced to a relatively small number:

- Production of defects due to the interaction of energetic particles with the atoms of the material;
- Diffusion of point-defects and their clusters, and their interaction with solute atoms distributed in the matrix, with the subsequent enhancement or induction of segregation and/or precipitation;
- Formation of clusters of point-defects and complexes that involve both these and the solutes, as a result of the balance between absorption of new defects and solutes;
- Emission of defects and solutes from clusters or other microstructural features;
- Recombination of point-defects with opposite defects (self-interstitials with vacancies and vice versa);
- Annihilation of defects at sinks, which generally correspond to pre-existing extended microstructural features, such as dislocations and boundaries between crystallites with different orientation.

The production of defects is the consequence of the collision of the impinging radiation particles with the atoms of the lattice and the sequence of atomic collisions that this can trigger (displacement cascade). These processes need to be studied using molecular dynamics simulations [32–34], of which microstructure evolution models take the outcome as an input, in terms of a spatial and generally localised distribution of point-defects and their clusters (primary damage state). Databases of cascades have been produced for several materials[1] and can be used directly as input to describe primary damage as a function of cascade energy.

For the purpose of correctly introducing the primary damage that is produced in the material, the primary knock-on atom (PKA) spectrum should be explicitly known or implicitly deduced from the knowledge of the energy spectrum of the impinging particles (neutrons, ions, electrons, …). The PKA spectrum is the number of atoms per unit time and volume that receive a given energy (PKA energy) from the impinging particle in the specific irradiation that one wants to simulate. It can be calculated with suitable codes and approximations from the knowledge of the neutron [35] or ion [36,37] flux as a function of energy. By subtracting from the PKA energy the energy that goes into electron excitation, one can deduce the corresponding cascade energy, which is responsible for the number of defects that are created [38]. With this information, supposing that cascades of all possible energy values are available from the database[1], the correct distribution of primary damage in space and time can be introduced.

In practice, the knowledge of the number of displacements per atom (dpa) that have been accumulated and the irradiation time, or alternatively the dpa-rate (dpa/s), are often sufficient to tune the cascade spectrum. When experimentalists evaluate the dpa that correspond to the irradiation they performed, they generally use the Norgett-Robinson-Torrens (NRT) model [39]. In [40] a revision of the dpa concept has been proposed, which will hopefully become commonplace in the future. In this revision, the dpa definition takes into account recombination and ion beam mixing effects that occur during the cascade, thereby making the dpa more physical. However for the moment the NRT model remains the most frequently used, which was definitely used in all past experiments. In this model, the number of displacements per cascade of given energy E, $n_d(E)$, is evaluated as:

$$n_d(E) = \frac{0.8E}{2E_d} \qquad (1)$$

Here E_d is the threshold displacement energy, i.e. the minimum energy needed to produce a stable defect (Frankel pair), which is 40 eV by standard in α-Fe [40]. Even if now a more reliable value for this parameter has been obtained by DFT [41], if the results of the simulation are to be compared with experiments as functions of dpa, the latter needs to be estimated in exactly the same way as in the experiments. Thus, the knowledge of the experimental dpa and dpa/s can be used to select, from a database of previously simulated cascades, those that produce the equivalent damage (according to the NRT model) at the equivalent rate, even if not all energy values are covered in the database. The effect that a specific choice of cascade database and cascade energy may have on the results are discussed in [8,42,43]. These studies show that the specific description of the primary damage state does affect the microstructure evolution that the model predicts; however, the dominant effect is clearly given by the parameters that govern the mobility and stability of defects [42], which are the focus of this review. For this reason, here we shall not deal any further with the issue of modelling damage production in microstructure evolution models, taking for granted that suitable molecular dynamics cascade databases are available and are used as correctly as possible.

Cascades are almost instantaneous, strongly localised processes, also from a microscale standpoint (few picosecond duration, few nanometer extension), see e.g. [32–34,44] and references therein. In addition to producing point-defect clusters, cascades may also produce solute athermal redistribution and formation of complexes involving solutes and point-defects at the end of the cooling phase in alloys, partly driven also by thermodynamic effects [45], and enhanced in case of athermal cascade accumulation [46]. However, the diffusion of defects, the formation of clusters and complexes with solutes, their dissociation and the absorption of defects at sinks occur mostly over a wide range of time and space scales [44]. Diffusion and dissociation are either thermally activated processes, with characteristic activation energy, or processes that occur spontaneously within a certain distance. As will be shown, assuming that the mechanisms that determine the details of these processes are sufficiently well understood and reflected in the model, the parameters that determine quantitatively the rate of these processes are:

---

[1] https://cascadesdb.iaea.org/

- Attempt frequency and activation energy for the migration of point-defects and their clusters, including the possibility that they form complexes with solutes that will influence their mobility;
- Attempt frequency and activation energy for the emission of defects from clusters (or from other microstructural features, if relevant);
- Distance of interaction between microstructural features and outcome of the interaction.

The difficulty with assigning a value to these parameters is that they depend on several variables, namely nature and type of the defect, its geometrical features, its diffusion mechanism, its size and composition, and its local environment as well. Sometimes these parameters may also depend on temperature and be influenced by magnetic properties, although in general the temperature dependence and other effects are all included in the transition state theory approach and in effective parameter values. The phase space of possibilities, especially when including solute atoms, becomes quickly combinatorially large. However, in order for the model to be applied, a specific value needs to be assigned to all and each of these parameters, whether known thanks to intensive DFT calculations or estimated on the bases of educated guesses. It is therefore easy to understand that the endeavour of defining a set of parameters that is sufficiently complete, physically defendable and practically applicable is a tough one. Unsurprisingly, it took years of studies, developments and calculations to reach a level of detail in the accepted knowledge that allows reasonably reliable microstructure evolution models to be produced and applied to realistic situations, for materials of technological interest such as Fe alloys. Many of these studies will be referenced in the unfolding of this work.

In this paper, we collect the sets of parameters that have been produced and used in the literature, putting them in a consistent framework, explaining their origin and, as much as possible, assessing the related uncertainty. They are compared and discussed in order to evaluate the impact of the choice and to select ready-to-use sets (given in the Supplementary Material), accompanied by all the theoretical and practical recommendations for their use. This is done here by focusing on pure Fe. Future papers– parts II and III - will address the role of, and parameters for, some solute atoms of specific interest, and how they can be implemented.

It is important to emphasise that the interaction of radiation defects with solutes, both of interstitial (e.g. C atoms) and substitutional (e.g. Cr, Cu, Ni, Si, Mn, P, …) nature, is crucial to properly understand and correctly simulate the microstructure evolution under irradiation in Fe. Pure Fe is indeed an abstraction: even in the purest material some impurities will exist and their presence will largely determine the kind of microstructure evolution that is observed with suitable experimental observation techniques. In purposefully alloyed Fe the presence of solutes of specific nature is, on the other hand, well-known to influence significantly the microstructure evolution, as a result of the interplay between radiation-induced effects, especially interaction between radiation defects and solutes, and thermodynamic driving forces. Thus a simulation in completely pure Fe, without any even simplified mechanism of trapping of defects due to the presence of solutes and other microstructural features, is doomed to predict a wrong microstructure evolution, irrespective of how correct the mechanisms and parameters may be, because hardly any experiment can claim absolute purity. Yet, an appropriate set of parameters for the description of the mechanisms that occur in pure Fe remains the necessary prerequisite for correct microstructure evolution simulation, in either relatively pure Fe or in Fe alloys.

The structure of this paper is as follows. We first describe the physics of radiation defects, with specific reference to iron (even though many aspects are general to other metals, particularly body-centred-cubic, bcc, metals), and introduce the fundamental equations that underlie OKMC-type microstructure evolution models, introducing the quantities of importance to parameterise the model. Next, we review for each class of parameters the values and choices that have been reported in the literature. As a conclusion, the areas where better parameters and further studies are needed are highlighted. In the Supplementary Material, recommended parameter sets are proposed.

Fundamental ideas to model radiation damage evolution in pure Fe

Configurations and general properties of point-defect clusters in Fe

Generally, the following are the defects considered in pure Fe:

1. Vacancies and vacancy clusters: Vacancy clusters in Fe are considered to be voids, since these are the most energetically favourable configurations for most sizes, according to simulations with different empirical potentials at 0 K [2,47,48]. Simulations show that, when damage is produced very close to the surface (keV ion implantation) [49], as well as when denser cascades are formed [50], large (few nanometre diameter) $\langle 1\,0\,0 \rangle$ vacancy loops can be formed by cascade collapse, in the former case due to self-interstitial depletion towards the surface. Cascade overlap also seems to enhance this possibility [51]. This is consistent with the results of early experiments of irradiation with heavy ions [52]. Simulation also suggests that $\frac{1}{2}\langle 1\,1\,1 \rangle$ vacancy loops, though unstable, may be formed and rapidly migrate to surfaces [48,53], before any transformation to voids occurs. Moreover, small clusters of around 10 vacancies are more stable in planar than volumetric configurations [54,55]. However, all these are exceptions and the most common vacancy clusters are in practice cavities. The dissociation and migration of small vacancy clusters has been widely studied statically using DFT and EIP [55–58], while only the latter have been used in the case of large clusters [54]. Molecular dynamics (MD) simulations would take prohibitively long times to describe vacancy cluster diffusion and dissociation, but atomistic kinetic Monte Carlo models with EIP can be used for dynamic studies of this type, see [59,60] and references therein. Vacancy clusters migrate in 3D as a consequence of several vacancy jumps that lead to the effective displacement of the cluster centre of mass. In the limit of large sizes, the motion of vacancy clusters (approximately spherical cavities) proceeds via migration of the atoms and thus of the vacancies on the internal surface of the cavity. Dissociation occurs via emission of single vacancies and the energy values involved in cluster migration and vacancy emission are similar, as will be seen. Because of the low mobility of vacancy clusters, it is often implicitly or explicitly assumed that only those with up to 4 vacancies can migrate [1–9,12,14,57], even though, as will be seen, nowadays there is relatively good knowledge of vacancy clusters migration parameters up to large sizes and this knowledge is expected to be important for high temperature simulations.

2. Self-interstitial atoms (SIA) and their clusters: Based on knowledge that was already widespread in the early 1990 s [61,62], two types of migration paths were considered since the early times of OKMC simulations, one-dimensional (1D) for self-interstitial clusters with planar loop shape and three-dimensional (3D) for the single self-interstitial, with different values for the migration energies in each case. Based on the most recent information, self-interstitial clusters in Fe can be grouped into four categories (Fig. 1 shows an example of each one of these groups of self-interstitial type defects): small clusters formed by parallel dumbbells, small clusters formed by non-parallel dumbbells, $\frac{1}{2}\langle 1\,1\,1 \rangle$ loops and $\langle 1\,0\,0 \rangle$ loops.

   A) Small clusters (<5 defects) are made of $\langle 1\,1\,0 \rangle$ parallel [63,64,65] or non-parallel [65,66] dumbbells. When in parallel configuration, these small clusters migrate in 3D, with energy on the order of 0.3–0.4 eV, as suggested by static (DFT and EIP) [7,57,65,67,68] and MD studies [63,64], as well as from experiments [62,69,70]. The non-parallel configurations, in contrast, some of which are often denoted as C_{15} clusters [71,72] (the non-parallel clusters include the C_{15} family, but there are non-parallel

clusters that do not create any local C_{15} crystallographic structure), are largely, though not completely, immobile and still represent an open problem, because their properties are not satisfactorily well known, yet. The reason for this lack of knowledge is that they are correctly identified as the most stable configurations only in DFT calculations [66] and many possible configurations may exist [66,71,72], while interatomic potentials generally favour parallel dumbbell configurations [65]. This limits the reach of the studies that can be performed, so for example not all possible configurations are known, even less are the unfaulting energy values known (we call *unfaulting* the mechanism whereby the non-parallel cluster evolves to a parallel, glissile configuration). The only explicit calculation of this quantity seems to have been performed with an EIP and for only one cluster [73]. Finally, it is not entirely clear which fraction of self-interstitial clusters is produced in parallel and non-parallel configuration in displacement cascades [14,71,74,75,76] and which role cascade overlap may play [77]. As a consequence, it is not simple to introduce explicitly these cluster configurations in microstructure evolution models and their role is therefore so far most often introduced indirectly, through effective parameters.

B) As clusters increase in size, the most stable configuration is that of $\frac{1}{2}\langle 111 \rangle$ loops [78–81], which migrate almost athermally by 1D glide along the direction of their Burgers vector, i.e. with migration barriers of $\sim$ 0.1 eV or less [3,53,63,64,68,81–84]. This glide occurs according to a mechanism that can be described either using the independent crowdion model [85], or as kink pair formation and propagation along the loop edge [81]. Experimentally, $\frac{1}{2}\langle 111 \rangle$ loops are regularly observed in iron under neutron [86–92] and also ion [93–98] irradiation. In addition, $\langle 100 \rangle$ self-interstitial loops are experimentally observed, as well [91–102]. The $\langle 100 \rangle$ loops represent the dominant majority whenever the irradiation is performed in relatively pure Fe, with neutrons, at or above 290 °C (operating temperature of most nuclear power reactors) [91,92,100–102].
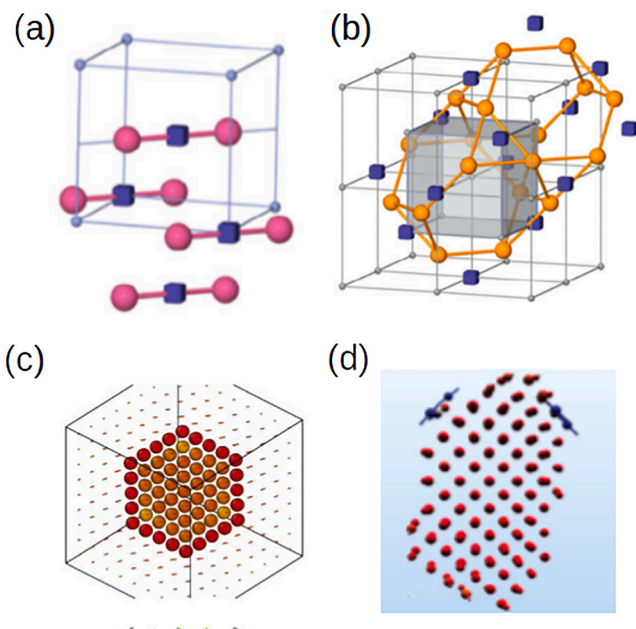
However, contrary to their expected higher stability with increasing temperature [79], $\langle 100 \rangle$ loops are also observed to form at (very) low temperature under ion [91,98] and electron [103] irradiation. Very refined electron microscopy experiments [103,104] show that all loops exhibit 1D motion, but, while $\frac{1}{2}\langle 111 \rangle$ loops start gliding at 450 K, $\langle 100 \rangle$ loops do so only above 770 K, i.e. $\langle 100 \rangle$ loops have higher migration energy. Interestingly, the experimentally-deduced migration energy of $\frac{1}{2}\langle 111 \rangle$ loops, ~1.3 eV, is an order of magnitude higher than the simulation value, ~0.1 eV. This difference is ascribed to the effect of the presence of impurities. A consistent estimate for the migration energy of $\langle 100 \rangle$ loops would be ~2.0 eV or higher (see section 2.5). However, for these loops no reliable calculation of this migration energy exists to date, so $\langle 100 \rangle$ loops are often considered as immobile in models, which is likely to be a good approximation. This very different mobility, perhaps in combination with the stability reversal [79], may explain why $\langle 100 \rangle$ loops are more frequently observed at higher irradiation temperature, when $\frac{1}{2}\langle 111 \rangle$ loops more effectively glide away to sinks. A gradual increase in the ratio between the two populations has been reported based on ion irradiation experiments [105]. Several mechanisms have been proposed for the formation of the less stable $\langle 100 \rangle$ loops. Simulations have shown that, by growing in size, C_{15} non-parallel clusters can transform into $\langle 100 \rangle$ loops, as well as into $\frac{1}{2}\langle 111 \rangle$ loops [106,107], or perhaps mainly into $\frac{1}{2}\langle 111 \rangle$ loops [76]. This is therefore a possible path for $\langle 100 \rangle$ loops formation. Another mechanism that may explain the appearance of $\langle 100 \rangle$ loops is the reaction between two $\frac{1}{2}\langle 111 \rangle$ loops [26,106,107,108]. Finally, spontaneous self-transformation with Burgers vector change has been observed experimentally [103]. Most OKMC models consider in practice only two types of self-interstitial clusters, 3D migrating clusters with sizes up to 4 defects, and fast 1D migrating clusters for larger sizes [1–11,15–21]. Sometimes the migration energy is tuned to effective values, which translate the existence of two types of clusters with very different mobility [10,11,15–21], occasionally assuming that self-interstitial clusters above size 4 are immobile [57]. Only a few models so far included explicitly the distinction between $\frac{1}{2}\langle 111 \rangle$ and $\langle 100 \rangle$ loops [12,14] and to our knowledge so far none explicitly treated C_{15} types of clusters. Overall, it is clear that there are still several unknowns concerning self-interstitial clusters, which too often oblige modellers to introduce mechanisms and parameters for these defects that are based on educated guesses more than actual knowledge.

Diffusion coefficient and its generalization to emission

The diffusion coefficient of a defect can be expressed as an Arrhenius-type law in the following manner [110]:

$$D(T) = D_0 exp(-E_a/k_B T) \tag{2}$$

where D_0 is the diffusivity pre-factor which includes the defect formation and migration entropy, E_a is the activation energy of the defect for diffusion, T is the temperature and k_B is the Boltzmann constant. It is important to stress that, in the absence of irradiation, the activation energy includes also the formation energy of the defect, but here we assume that the defect has been already created, thus this contribution should be removed and only the migration energy remains. D_0 can in turn be expressed in terms of the distance of a single jump, d_j, the attempt frequency of migration, ν_m, and the correlation factor, f_C, which may be temperature dependent if the diffusion mechanism changes with temperature (this might be true for self-interstitials or for point-defect clusters):

Fig. 1. Examples of the four different types of self-interstitial clusters in Fe: (a) $\langle 110 \rangle$ self-interstitial cluster with 4 defects, from [72], reprinted with permission from Elsevier; (b) C_{15} cluster with 4 self-interstitials [72], also reprinted with permission from Elsevier; (c) a 37 self-interstitials $\frac{1}{2}\langle 111 \rangle$ loop, from [109], also reprinted with permission from Elsevier. (d) $\langle 100 \rangle$ loop, reprinted with permission from [26], copyright 2013 by the American Physical Society.

$$D_0 = f_c(T) \frac{d_j^2}{2\zeta} \nu_m \qquad (3)$$

Here ζ is the dimensionality of the migration (1, 2 or 3 for one-, two- or three-dimensional motion). In addition,

$$\Gamma(T) = \nu_m exp(-E_m/k_B T) \qquad (4)$$

is known as the jump (or migration) frequency, with E_m the migration energy of the defect and ν_m its attempt frequency of migration. In the case of pure random walk, there are no correlation effects, i.e. $f_c(T) \sim 1$; moreover, given that the defects have been already created, $E_a \sim E_m$. Therefore, under the hypothesis of uncorrelated motion, the diffusion coefficient for any defect can be considered for practical purposes as directly proportional to the jump frequency:

$$D(T) \cong \frac{d_j^2}{2\zeta} \Gamma(T) \qquad (5)$$

Some models use $D(T)$, others use $\Gamma(T)$, but eq. (5) allows the switching from one to the other and both can in practice be considered as known when the migration energy and the attempt frequency are known. Therefore, these two parameters, E_m and ν_m, are all we need to describe defect mobility. In the case of point-defect clusters, both depend on the type of cluster (vacancy or self-interstitial), its configuration (planar or volumetric, parallel or non-parallel dumbbells in the case of SIA clusters, Burgers vector for loops, …) and the number, n, of point-defects in the cluster, i.e. for a given type of cluster of defined configuration, $E_m = E_m(n)$ and $\nu_m = \nu_m(n)$.

For practical use in OKMC models, the concept of diffusivity can be generalized to the process of emission of a defect from a parent cluster, typically emitting a single point-defect. This process is called dissociation and in this case the diffusion distance is very short, but it is useful to extend to this case the formalism of eqs. (2)-(5) for those models that work with diffusion coefficients rather than with jump frequencies. In the expression of this effective diffusivity, the activation energy of interest, the dissociation energy E_d, can be approximated as the sum of the energy that is necessary for the defect to be detached from the cluster, E_b, binding energy, and the migration energy of the defect emitted, $E_{m,e}$. While the last one only depends on the type of (single) point-defect emitted, the other two depend on the type and number of point defects in the cluster, n, i.e. the size of the cluster:

$$E_d(n) = E_b(n) + E_{m,e}(1) \qquad (6)$$

The corresponding effective diffusivity for emission is therefore:

$$D^e(T) = D_0^e exp\left(-\left(E_{m,e} + E_b\right)/k_B T\right) = D_0^e exp(-E_d/k_B T) \qquad (7)$$

And the product:

$$\Gamma^e(T) = \nu_e exp(-E_d/k_B T) \qquad (8)$$

is the frequency of emission, which is related to the effective diffusivity for emission by an equation like eq. (5), the pre-factor D_0^e being expressed in a similar way as in eq. (3), after replacing ν_m with ν_e, which is the attempt frequency of emission. Both E_b and ν_e are functions of the type, configuration and size n of the emitting cluster. These two are the functions that in practice we need to know to describe cluster dissociation.

If other types of dissociations of a cluster are possible, in addition to the emission of a single point-defect, the corresponding reactions can be introduced and the definition of dissociation energy generalized, becoming a function also of the size of the emitted cluster. However, in general this possibility is disregarded as energetically unfavourable, except in the case of point-defect/solute complexes, which may emit a point-defect/solute pair (not relevant for pure Fe).

Overall, migration and emission are thermally activated processes, that are described in a transition state theory framework [111], i.e. using Arrhenius-like functions to express the frequency of events, with characteristic activation energy values that are independent of temperature.

Binding energy

As explained above, the binding energy of point-defects to clusters of different types and configuration as a function of size is necessary to describe emission. If $E_f(n)$ is the formation energy of a certain type of clusters of n point-defects, the binding energy $E_b(n)$ of a single point-defect to it is defined as the difference between the energy of the cluster after removing one point-defect and before doing so:

$$E_b(n) = E_f(n-1) + E_f(1) - E_f(n) \qquad (9)$$

The name binding energy is also often used to denote the energy difference between all defects in a cluster and the same number of defects isolated (*explosion* energy, or total binding energy):

$$E_{b,tot}(n) = nE_f(1) - E_f(n) \qquad (10)$$

This total binding energy is generally not directly used as a parameter in OKMC simulations, but it is a useful quantity, because it is easy to see that the following relationship holds:

$$E_b(n) = E_{b,tot}(n) - E_{b,tot}(n-1) \qquad (11)$$

In the limit of large n, therefore, one can write:

$$E_b(n) \rightarrow \frac{dE_{b,tot}(n)}{dn} = E_f(1) - \frac{dE_f(n)}{dn} \qquad (12)$$

As shown later on, the formation energy of a cluster scales as a power $2/3$ or $1/2$, thus the derivative is always positive and tends to zero for large sizes. This is so because the stability of a cluster implies that its formation energy should be less than the sum of the formation energy of each point-defect, i.e. $E_{b,tot}(n)$ is always positive, meaning that the increase of $E_f(n)$ must follow a less-than-linear trend. Thus eq. (12) shows that the binding energy of the single point-defect to a cluster is always less than the formation energy of the single point-defect. In the case of vacancies, for example, it is intuitive that the emission of a vacancy from an infinitely large cavity, i.e. from a free surface, is equivalent to its formation, thus it makes complete sense that the asymptotic value of the binding energy should be the formation energy.

Sinks, traps and capture radii

As mentioned, under irradiation defects are produced, diffuse and, when meeting, may recombine (if of opposite type) or cluster. The recombination is the simplest reaction in which defects disappear, by being absorbed by each other, i.e. a vacancy disappears on a self-interstitial and vice versa. Defects can also disappear at microstructural features such as dislocations and grain boundaries, as well as any other type of interface between different crystal orientations (lath or twin boundaries), or between incoherent phases in alloys, or layers in multi-layered materials, or at free surfaces. These are classically called sinks for point-defects and their clusters. Differently from migration or dissociation events, events such as recombination, clustering and absorption at sinks have in common the feature of occurring spontaneously, athermally, whenever the two objects involved find themselves at a distance where they interact so strongly with each other that the reaction becomes unavoidable. The detailed mechanisms of the reaction may be quite complex at the atomic level and occur through a series of strongly biased diffusion jumps and reconfigurations, in some cases with a delay that makes them not instantaneous. Yet, when the capture of an object by the other occurs, the outcome of their reaction is established. Because of this idea of one object irreversibly capturing another one, the distance below which the interaction spontaneously occurs is often called *capture distance*. Since, moreover, in most cases defects are assumed to have a spherical shape, or sometimes cylindrical or toroidal, this distance is generally a radius, hence the common expression *capture radius*. It is thus necessary to define capture radii for all possible

reactions of recombination, clustering or absorption by sinks. This capture radii will depend on the two interacting objects, their type, inherent configuration and, if relevant, their size.

The concept of capture radius is clearly a strong simplification. In reality defects "see each other" from a certain distance, which can be fairly large, because of their strain field, i.e. because of the distortion they create in the lattice, which gives rise to attractive or repulsive elastic interactions that depend on the two defects involved, their geometry and their mutual orientation. Some OKMC schemes have therefore implemented elastic interactions, which enter as a bias in the migration energy, removing the need to define capture radii [112–118], at least for those defects for which an analytical expression of their elastic field and their elastic interaction can be obtained. In the description of how mobile defects interact with dislocations, for example, it is certainly crucial to introduce a description of the elastic strain field, which may be attractive or repulsive depending on type of dislocation and approaching defect in specific regions of space [119–121]. The explicit introduction of elastic interactions in an OKMC scheme allows in this case the formation of non-uniform distributions of dislocation loops, such as rafts or clouds around dislocations that are often observed experimentally [89,90,93,102], to be described in the simulation [112,114].

However, the introduction of elastic interactions has some shortcomings. First of all, it is not always obvious how to describe the elastic interaction between all types of radiation defects. Only fairly recently have closed form expressions been obtained for the elastic interaction between radiation defects (loops and cavities) located at larger distance than their size from each other [122] or for the stress and strain field evaluated at sufficiently large distance from a defect of any structure [123]. These elasticity theory expressions enable the removal of the concept of capture radius, but may fail at the atomic level or in alloys where complex defects that contain both point-defects and solutes, in a variety of irregular arrangements, are formed. In fact, even the sheer presence of solute atoms may introduce significant local deviations in the distributions of strains and stresses [124].

Another issue related with the introduction of elastic interactions in OKMC models is that they are of long range type, thereby obliging in principle to refresh the list of events of all defects in the whole box at each step. This introduces an unavoidable additional computational burden of some significance, especially when the density and size of mutually interacting defects is large. Moreover, the larger the simulation volume, the more significant this additional burden is expected to become. Since the actual interaction energy becomes negligibly small for large distances, it is possible to introduce a cut-off radius. This, however, is itself a sort of capture radius that needs to be chosen based on some more or less empirical criterion. Its introduction might eventually even offset the physical advantage of introducing elastic interactions. Estimates made by one of the authors in a cubic simulation volume with side of 250 lattice parameters and including only dislocation loops suggest that the computing time when the elastic interactions are switched on (with a cutoff) may be 6–7 times longer, although the difference reduced significantly with increasing loops size. For these reasons, so far elastic interactions have been introduced only to study very specific issues, for example the creation of heterogeneous distributions of defects in presence of either locally high densities of defects (cascade ageing) [113] or dislocation lines/loops [112,114], or else the evaluation of the effect of elastic interactions on the sink strengths (the inverse of the square of the mean diffusion distance before a defect is absorbed by a sink) of extended defects [115–118]. These studies are useful because they allow convenient capture radii and relevant biases to be derived, for use in simpler models, so that these can implicitly embody, as correctly as possible, the extension and features of the elastic strain field associated with a given object, when interacting with the strain field created by other objects, as described below.

Irrespective of whether or not a model includes a description of elastic interactions, there exists yet another problem. As well as clusters of point-defects do not only absorb, but also (re-)emit defects (generally only single point-defects), likewise complex microstructural features that act as sinks, such as dislocations and crystallite boundaries, may be such that certain types of defects do not disappear in them for good: they remain "parked" there and can be (re-)emitted later, at the price of a given activation energy (thermally activated processes). If this happens, it is customary to talk of *traps*, i.e. objects that temporarily stop defects that enter their orbit, until re-emission. However, the fact that extended sinks such as dislocations and crystallite boundaries may act both as sinks and traps and (re-)emit defects creates difficulties. In most if not all microstructure evolution models, the internal structure of these microstructural features is, on purpose, completely disregarded, due to its inherent complexity: they are simply sinks, i.e. places with a given geometry where objects disappear. Furthermore, the volumes used in OKMC-type simulations are generally much smaller than a grain, thus no grain can be fully included in the simulation box, while also introducing dislocation lines corresponding to sensible density values may be problematic [125]. The introduction of elastic interactions allows the model to describe how migrating defects approach these extended microstructural features, without the need to introduce a capture radius, but clearly this information is not enough. The final fate also needs to be known: will the defect be absorbed or trapped [119]? May the defect be eventually (re-)emitted? Small defects will likely be absorbed by dislocations lines (up to which size? [119]), but larger defects, e.g. dislocation loops, may be effectively trapped [112,114,126]. Trapped defects may later be absorbed (spontaneously or upon straining), or they may remain trapped, either forever or for a while if there is a possibility to be released. Grain boundaries create a less well defined and much more variable strain field than dislocations, but they also may be attractive to certain defects, inducing for example accumulation of loops close to them [127], or act as sinks/traps for point-defects and then re-emit them [128].

Thus, a proper description of the role of dislocations and grain boundaries requires *a priori* not only the introduction of elastic interactions in OKMC, but also a detailed knowledge of how a specific extended defect interacts with an incoming migrating defect at the atomic level, through atomistic processes. On-the-fly [24–27] or hybrid [60,129] models are being developed to address among others these situations. This, however, is not the objective of OKMC models, and microstructure evolution models in general, which on the contrary try to detach themselves as much as possible from the atomistic details, in order to reduce the computing time and enable long irradiation processes to be simulated. Finding a satisfactory compromise is not simple, but capture radius-based approximations are a way to do so, if associated with the use of classical expressions of sink strengths from the rate theory, for sinks of different geometries (absorbing spheres, arrays of parallel dislocation lines, loops, spherical grains, …) and for defects migrating according to 3D or 1D paths [125,130–137]. These sink strengths depend on the relative extension of the sink, for instance the sink strength of dislocations is proportional to their density [125,131,132], while the sink strength of a grain boundary is inversely proportional to the square of the grain radius (in a spherical grain approximation) [134,135].

Specifically, it is possible to "replace" the sink effect of dislocation lines of a given density with uniformly distributed spherical absorbers. Once the number density, n_s, of these absorbers is fixed, their radius, r_s, can be obtained in such a way that their sink strength is the same as the one of an array of parallel dislocation lines, with given density ρ_d; or else a reasonable density and radius can be traded off. This can be done by equating, for example:

$$4\pi n_s r_s = \frac{2\pi\rho_d}{ln\left(\frac{1}{\rho}\right)} \tag{13}$$

Here $\rho = r_d\sqrt{\pi\rho_d}$, where r_d is the capture radius of the dislocation. The

Table 1

Correspondence between activation energy, E_a (eV), and activation temperature, T_a (for convenience given in both K and °C), using as criterion two different critical frequencies, 1 and 10^4 s^{-1}.

E_a (eV)	T_a (K)		T_a (°C)	
	$\Gamma_c = 1.0$ s^{-1}	$\Gamma_c = 10^4$ s^{-1}	$\Gamma_c = 1.0$ s^{-1}	$\Gamma_c = 10^4$ s^{-1}
0.3 (migration single SIA)	115	167	−158	−106
0.6 (migration single vacancy)	231	333	−42	60
0.9 (migration of C in Fe)	346	500	73	227
1.2 (migration of void)	462	667	189	394
1.5 (high activation*)	577	833	304	560

*High with respect to processes of defect migration, typically corresponds to dissociation of highly stable defects

left hand side of eq. (13) is the simplest expression for the sink strength of a population of spherical absorbers [130,135], while the right hand side is the simplest expression for the sink strength of an array of parallel dislocation lines [132]; other, more complex expressions can also be used for the latter [125,130], however they are all equivalent in the limit of small sink volume fraction. The studies performed in [125,130] demonstrate that the sink strength theoretically deduced from the resolution of diffusion equations is well reproduced by OKMC type models, provided that certain care is taken with the simulation setup. The problem is the knowledge of the capture radius of the dislocation line, r_d, a quantity that depends on the defect that is captured by the dislocation (for example it is larger for self-interstitials than for vacancies), as well as from other variables, including temperature. It needs to be chosen based on atomistic, dislocation dynamics or other types of calculations and considerations [114–119,138,139], or else suitably tuned, in all cases with a dose of arbitrariness. It is possible to work with an explicit bias, i.e. to set $r_s^\delta = r_s Z_\delta$, where δ = I,V (self-interstitial or vacancy), with $Z_V = 1$ and $Z_I > 1$, typically 1.15–1.2, although higher values are also possible. This bias is itself a way to account for elastic interactions between point defects and dislocations. It will thus be necessary to introduce two families of absorbers, one for vacancy-type defects and one for self-interstitial-type defects. It must also be noted that, strictly speaking, the radius r_s assumes a point-like migrating defect, without any associated radius or volume, thus a decision should be made to manage the fact that generally defects have an associated volume. In [11] the following, simplified equation was used to obtain r_s^δ, which takes into account that the radius of the absorbed defect needs to be removed from the spherical absorber radius:

$$r_s^\delta = \frac{\rho V}{4\pi n_s} Z^\delta - r_1^\delta \tag{14}$$

Here V is the volume of the simulation box (thus the radius of the spherical absorbers is simulation-volume dependent) and r_1^δ is the radius associated with either a single vacancy or a self-interstitial (see section 3.5). In the same work it was also assumed that only single point-defects or small clusters thereof are absorbed by sinks, to mimic the fact that dislocations appear to be decorated by loops, which are thus most likely not absorbed in most cases, but trapped instead. However, clearly this approach does not allow non-uniform loop distributions to be simulated, it simply does not remove the loops that in the microscope appear close to dislocations and are counted in when determining their total density. A proper account of heterogeneous loop distributions requires either the generalized introduction of elastic interactions as discussed above, or attempts at treating in a simplified, but more realistic, way the sink role played by dislocations, as suggested in [119].

The sink strength of grain boundaries, on the other hand, is best taken into account assuming spherical grains and working with two sets of coordinates that should be associated with the defects. One set represents the actual position inside the simulation volume, generally with the shape of a parallelepiped, and is subject to periodic boundary conditions (a defect that leaves the simulation volume re-enters it from the opposite side). The other set is a radial coordinate that represents the distance from the center of the grain. The radial coordinates are initially randomly assigned to any newly created defect and then updated without taking into account the periodicity. If and when the radial distance of a defect becomes more than the grain radius, this defect suddenly disappears. It has been demonstrated that this algorithm reproduces well the theoretical sink strength of grain boundaries, assuming spherical grains [130].

Finally, similarly to spherical absorbers, spherical traps may also be introduced in models to replace the effect of solutes, e.g. carbon atoms, when the detailed description of solute/defect interaction is not sufficiently well known. Traps are also introduced to take care for the presence of unknown microstructural features that reduce the effective mobility of radiation defects by acting as traps, including impurities and dislocations [2–11,15–21]. Clearly, however, the values of the trap capture radius and of the de-trapping energy that are involved suffer from a degree of arbitrariness and need to be calibrated.

Correlation between activation energy and activation temperature

It is useful to associate with thermally activated events of energy E_a a temperature of activation T_a, above which the event becomes actually activated, i.e. it does influence the evolution of the system. Along the lines of what is explained in [140], an event can be said to be activated when its frequency, Γ_c, is equal to, or higher than, a critical value. To take into account different situations, e.g. different dose rates, here we choose two representative critical rates, namely 1 Hz and 10^4 Hz. By imposing that the migration or dissociation frequency in eqs. (4) or (8) should equal these values, with attempt frequency $\nu = 10^{13}$ s^{-1} (Debye frequency in Fe), a simple linear relationship is obtained between activation energy and temperature of activation, $E_a = \alpha T_a$, with $\alpha = 0.0026$ for $\Gamma_c = 1$ s^{-1} and $\alpha = 0.0018$ for $\Gamma_c = 10^4$ s^{-1}. Table 1 shows the correspondence between activation energy and activation temperature using the two relationships and therefore criteria.

The values of activation energy that have been chosen in Table 1 roughly correspond to characteristic energy values for the migration of defects in Fe, as revealed by isochronous annealing recovery experiments [62], or as later shown in this work. Interestingly, the criterion $\Gamma_c = 1.0$ s^{-1} provides temperatures that correspond to the stages of recovery revealed in the mentioned experiments. The criterion $\Gamma_c = 10^4$ s^{-1} is suitable to assess the impact of event when the dose rate is high or to state that an event is not only activated, but in fact significantly frequent.

Parameters to model radiation damage evolution in pure Fe

In the following the data that exist on migration and binding energy values for different types of point-defect clusters in α-Fe, as well as the relevant attempt frequencies of migration and emission, are listed and discussed, providing functions for their dependence on size in view of extrapolation. The nomenclature used is as follows: V_n is a cluster of n vacancies and I-Tn is a self-interstitial cluster of type T (Burgers vector) that contains n self-interstitials. If no type label is included, it means that the same rule applies for all self-interstitial types (for example, binding energy of self-interstitial clusters).

Migration energy values for point-defect clusters in Fe

The migration energy of a cluster depends on its type, configuration and size, i.e. for a given type of cluster with a certain type of configuration is $E_m = E_m(n)$. Table 1a lists some values of migration energy of small clusters of vacancies and self-interstitials in Fe, as obtained from DFT calculations, including a few experimental values, as well. Here for the self-interstitials the reference configurations are parallel $\langle 110 \rangle$

Table 1a

Migration energy, $E_m(n)$, for small point-defect clusters in pure Fe. Values are denoted as DFT, Exp (experimental) and EIP (empirical interatomic potential), using in the latter case an atomistic kinetic Monte Carlo model for clusters. Values in italics are assumptions.

Species	$E_{m(n)}$ (eV)	Migration type	Refs.
V_1	0.64	3D	DFT [56]
	0.67		DFT [57]
	0.66; 0.68		DFT [58]
	0.54		DFT [55]
	0.55		Exp [141,142]
	0.57 ± 0.14		Exp [143]
	0.63		EIP [59]
V_2	0.62	3D	DFT [57]
	0.66		DFT-based AKMC [58]
	0.55		DFT [55]
	0.63		EIP [59]
V_3	0.35	3D	DFT [57]
	0.36		DFT [55]
	0.58		EIP [59]
V_4	0.48	3D	DFT [57]
	0.44		DFT [55]
	0.63		EIP [59]
$I \langle 1\,1\,0 \rangle$	0.34	3D	DFT [57]
	0.31		Exp [62,69,70]
	0.27		EIP [64]
$I \langle 1\,1\,0 \rangle\,2$	0.42	3D	DFT [57]
	0.42		Exp. [62]
	0.36		EIP [64]
	0.55*		DFT (P. Olsson, private comm. 2012)*
$I \langle 1\,1\,0 \rangle\,3$	0.43	3D	DFT [57]**
	0.16		EIP [64]
$I \langle 1\,1\,0 \rangle\,4$	0.43**	3D (?)	[68]**
	0.16		EIP [64]
	0.8***		[10]***

*Migration energy of the non-parallel configuration of the di-interstitial, possibly coinciding with the unfaulting energy.

**DFT calculations show that the threshold size for the cluster configuration to switch from a collection of $\langle 1\,1\,0 \rangle$ dumbbells to $\frac{1}{2}\langle 1\,1\,1 \rangle$ loops is 5 self-interstitials [68]. No information exists from DFT about the mobility of $I \langle 1\,1\,0 \rangle\,4$, so the same mobility as size $I \langle 1\,1\,0 \rangle\,3$ is assigned, assuming that the migration mechanism is the same, i.e. rotation and translation of parallel dumbbells (the mobility of $I \langle 1\,1\,0 \rangle\,2$ and $I \langle 1\,1\,0 \rangle\,3$ is also very similar). Molecular dynamics studies with EIP provide the same energy for both, although its value is about half.

***Here the assumption is that the effective migration energy for the tetra-interstitial is dictated by the unfaulting energy to transform the stable non-parallel configuration into the parallel dumbbell configuration. This energy, 0.8 eV, is only known from an EIP calculation in the specific case of the tetra-interstitial [73]. Further discussions of migration energy values for small self-interstitial clusters can be found in [10].

dumbbells. Although it is known that these clusters are more stable in non-parallel configurations (some of which are denoted as C_{15} [71,72]), knowledge on mechanisms and characteristic energy values for non-parallel clusters is too limited to be able to describe them explicitly. Their existence is taken into account in an indirect way and how this is done changes on a case by case basis and is still evolving.

A discrepancy exists between the migration energy for single vacancies and divacancies as obtained in relatively early DFT studies [56,57,58] and in [55], while there is agreement for V_3 and V_4. The value of [55] for the single-vacancy migration energy is closer to the experimental value [141–143] and stands out because most DFT and EIP calculations tend to provide values that are higher than 0.6 eV and often closer to 0.7 eV [58]. Using the precise value for the migration energy of single point-defects and small clusters is important if the model is expected to be compared with irradiation experiments performed at low temperature followed by annealing, for example resistivity recovery studies that identify the onset temperature of migration of single point-defects and their dimers, or other experiments of the same kind, such as in [62,69,70,141–143]. In contrast, for the simulation of radiation damage accumulation at room temperature, or higher, the description of the migration of large clusters, especially of self-interstitials, becomes the dominant factor, because single point-defect migration occurs with sufficiently high frequency to make the second figure after the comma essentially irrelevant. With this in mind, values can be rounded and one can say that, according to DFT and experiment, within uncertainty single and di-vacancy have essentially the same migration energy, ~0.6 eV, while the tri- and tetra-vacancy migrate with lower energy, ~0.4 eV. The single interstitial migration energy is ~0.3 eV, while clusters of up to 4 self-interstitials are likely to migrate with an effective energy value ~0.4 eV, although the doubt remains about the role of non-parallel configurations on this effective migration energy, which might be significantly higher (up to ~ 0.8 eV for the tetra-interstitial, $I \langle 1\,1\,0 \rangle\,4$, if it coincides with the unfaulting energy). We here recommend the use of these values, because they describe the same type of clusters (parallel ones) and avoid for example peaks of concentrations for clusters that are given an especially high migration energy (0.8 eV), as happened in [10,11]. Ideally, non-parallel clusters should be treated as a separate class with their own properties (fraction in cascades, unfaulting energy, …), but this is currently not possible because of the knowledge gaps that still need to be overcome. One option to effectively take into account the existence of immobile, or slowly migrating, clusters is to increase artificially the effective migration energy of small clusters, however this requires some calibration to be performed versus reliable experimental data. This type of approach has been used in the case of invisible clusters in [11], where an effective migration energy of 0.2 eV was assigned to self-interstitial clusters that are large enough to take a loop configuration, but are too small to be visible.
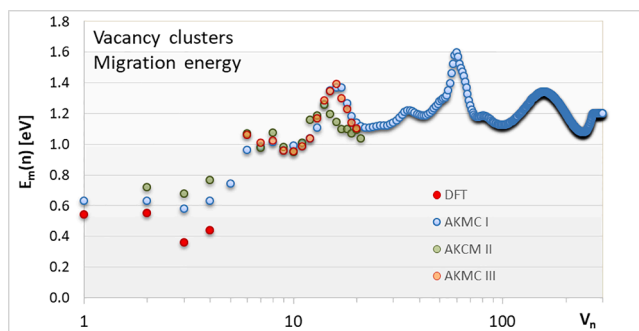
Table 1b

Migration energy values (E_m) typically adopted for large point-defects clusters in pure Fe.

Species	$E_m(n)$ (eV)	Migration type	Reference
V_n, $n > 4$	Immobile	3D	[57]
	Or AKMC values (Suppl. Mater.)		EIP [59]
$I \langle 1\,1\,1 \rangle\,n$, $n > 4$	$0.06 + 0.11/n^{1.6}$	1D	MD [3]
	0.2 (if invisible in TEM, i.e. $n < 60$–90)*;		[11]
	0.1 (if visible in TEM, i.e. $n > 60$–90)		[11]
	<0.1 eV, e.g. 0.05 eV		This work choice, based on [3,53,63,64,68,81–84]
$I \langle 1\,0\,0 \rangle\,n$, $n > 5$	Immobile	1D	Typical choice
	Or 0.9**		[11]

*TEM = Transmission Electron Microscope. Here the reasoning is that the nature of invisible clusters ($\langle 1\,1\,1 \rangle$, $\langle 1\,0\,0 \rangle$, C_{15}, …) is not known experimentally, thus the "average" migration energy will be higher than the migration energy of pure $\langle 1\,1\,1 \rangle$ loops, given that $\langle 1\,0\,0 \rangle$ loops migrate with much higher energy and C_{15} are immobile (but may transform into $\langle 1\,0\,0 \rangle$ and also $\frac{1}{2}\langle 1\,1\,1 \rangle$ [76,106,107]). However, the threshold energy for visibility is not unambiguously defined and can be taken between 60 and 90 self-interstitials.

**The migration energy of $\langle 1\,0\,0 \rangle$ loops is controversial. The value 0.9 eV employed in [11] was privately communicated by Y.N. Osetsky (ORNL), who had done MD calculations that were, however, never published.

Fig. 2. Vacancy cluster migration energy as a function of size. Most values are the results of AKMC studies from [59] (AKMC I), parameterised on the M03 interatomic potential [146], as well as from [60] (AKMC II and III, which differ because based on different reference DFT data sets used for the parameterization, respectively from [147;148]). The values from DFT for the first four clusters [55] are indicated, as well. Above size 250 a constant value 1.2 eV is used, which is the median of the AKMC I values between 10 and 250.

Concerning point-defect clusters of more than four point-defects, the most common migration energy values used in microstructure evolution models are summarised in Table 1b.

Most OKMC simulations assume that vacancy clusters with $n > 4$ are immobile. This can be an excellent approximation for simulations at low temperature, given that the migration energy of these clusters generally exceeds 1 eV (see Fig. 2). The advantage of assuming their immobility is that a whole lot of parameters can be forgotten about. This assumption also enables the use of computationally much faster rate equation models, which have difficulties to treat mobile species, to the extent that even the most advanced solving methods, which extend to large size defects and multi-component systems, in practice assume only single point-defects to be mobile, see e.g. [144,145]. It is, however, a very strong and questionable approximation, which becomes unjustified when temperatures of technological interest, from round 300 °C upward, are considered. At these temperatures, the jump frequency of objects that migrate with 1 eV is well above the $10^4 \, \text{s}^{-1}$ activation threshold (see Table 1). While these frequencies remain way too low for MD calculations, in [11] the values for migration energies of clusters were taken from atomistic KMC (AKMC) calculations [59]. These calculations were performed by tracing the mean square displacement of vacancy clusters and applying the standard expression for the diffusion coefficient. This reference study, denoted as AKMC I, was conducted up to 250 vacancies for a discrete number of clusters, using a neural network to predict energy barriers as functions of the environment (other vacancies) [59]. The neural network had been trained on barriers calculated with an interatomic potential denoted as M03 [146] and the resulting discrete diffusion coefficient data points were then interpolated using splines. These values are shown in Fig. 2 and compared with similar AKMC studies that were conducted on a smaller number of relatively small clusters [60], using significantly different procedures for the calculation of the energy barriers. Namely, these AKMC models used a standard barrier definition based on energy differences, calculated as sums of pair energy values fitted to available DFT calculations. Both earlier [147] and more recent [148] reference DFT values were used. These two AKMC models are denoted in Fig. 2 as AKMC II and AKMC III, respectively. In the same figure, also the most recent DFT values for vacancy cluster migration energy are indicated [55]. In the case of clusters of more than five vacancies, all AKMC models indicate that the migration energy oscillates in the range 0.9–1.6 eV, meaning that the jump frequency of sizeable vacancy clusters is low, but not completely negligible above 300 °C, depending on the specific size. The oscillations become dumped above 60 vacancies. This suggests a trend towards a specific migration mechanism (most likely surface migration), with a single activation energy value. Thus, above 250 the migration energy has been equalled to 1.2 eV, which is the median of the AKMC I values between size 10 and size 250. It is noteworthy

that the three AKMC models, although significantly different in the way the energy barriers are calculated, lead to extremely similar results. This gives a certain confidence that the values and the trends are robust. In particular, all predict the existence of at least one peak of migration energy values. These peaks correspond to specific cluster geometries that give high stability, typically fully filled shells of close neighbour vacancies, approaching the spherical shape, compatibly with the crystallographic structure. Two models predict the same peak in exactly the same position along the size axis. Therefore, these calculations show that monotonically growing functions of size are not suitable to interpolate the migration energy of vacancy clusters, because some cluster configurations are more stable and migrate with higher energy than larger ones. For instance, a cluster of about 50 vacancies migrates with ~1.5 eV, while a cluster of 90 vacancies with only ~1 eV. This depends on how easy it is for the atoms to migrate on the internal surface of the cavity, which depends strongly on the cluster configuration, until large sizes are reached that approximate free surfaces. It may be understood that clusters that, in their lowest energy configuration, complete a perfect sequence of (removed) atomic layers, thereby having facets on perfect crystallographic surfaces, will have more difficulty to migrate than clusters with extra vacancies on their facets. These types of processes are caught correctly by AKMC models, because these are *dynamic* models, i.e. they include the fact that the effective migration of a cluster is the result of several jumps of the vacancies, which make the cluster continuously change configuration. This way of performing the calculations is thus more representative of the overall migration process than, for example, DFT studies, in which by necessity the migration path has to be found via "manual search" through different possibilities, irrespective of the higher reliability of the barrier calculation. However, for small clusters DFT values are certainly a better reference, especially because it appears that the AKMC study is not able to catch the low migration energy value in the case of tri- and tetra-vacancy (not because of the method itself, but because of the limitations of the Hamiltonian that is implicitly used).

Even though DFT values are expected to be the best reference, in [10,11] for consistency the migration energy of small vacancy clusters was chosen to be the one coming from the interatomic potential, calculated by AKMC. Consistency may be important because often in OKMC simulations the relative difference between event frequencies plays a greater role than the absolute value, since it determines the relative rate of occurrence between competing processes. The corresponding AKMC energy values for small clusters are included in Table 1a, denoted as "EIP". The complete list of recommended migration energy values for vacancy clusters is given in the Supplementary Material.

Concerning self-interstitial clusters, as mentioned, loops glide in 1D along the direction of their Burgers vector. Of these, ½⟨111⟩ loops migrate almost athermally [3,53,63,64,68,81–84], thus the law of migration energy versus size proposed by Soneda and de la Rubia [3] (see Table 1b) has been used [4,5,8,14,113], or equivalently values on the order of 0.1 eV or less are chosen. In contrast, ⟨100⟩ loops are often considered immobile as their migration energy is known to be high, although its value is currently not precisely known (in Table 1b the value 0.9 eV is adopted based on a private communication of Yu.N. Osetsky, years ago). Models that use only one type of loop, without distinction of Burgers vector, assigned to these defects a sort of effective migration energy value. For example in [10] the migration energy for visible loops (n > 90) was set to 0.9 eV, because experimentally in Fe ⟨100⟩ loops are invariably observed in irradiation experiments performed at 300 °C or above [91,92,100–102,105], while for invisible clusters an effective value of 0.2 eV was found to provide good agreement with reference experiments.

It is clear that the parameter sets used for self-interstitial clusters are much more rudimentary and overall affected by higher uncertainties than in the case of vacancies. In particular, the parameter set will be unavoidably characterised by discontinuities and questionably chosen size dependences. Fig. 3 shows three examples of choice of migration energy values as functions of size and illustrates that a constant value of ~0.1 eV or smaller is an equivalent choice to using the law by Soneda and de la Rubia in Table 1b [3]. The parameters proposed in this work
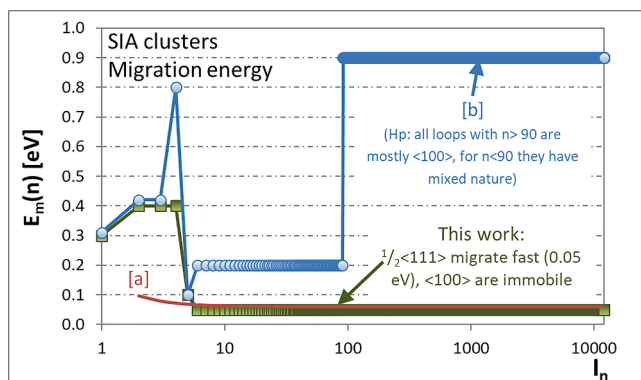
Fig. 3. Different choices of migration energy versus self-interstitial atom (SIA) cluster size, $E_m(n)$. The squares correspond to the choice made in this work (see Supplementary Materials for the tabulation). The curve [a] corresponds to the law given in ref. [3]: a constant value of ~ 0.1 eV or smaller is an equivalent choice to using that law. The circles [b] correspond to the choice made in ref. [10], where, as described, all loops with more than 90 SIA have been considered to have Burger's vector $\langle 1\,0\,0\rangle$ with migration energy 0.9 eV, while below this threshold an effective migration energy value of 0.2 eV has been chosen for loops.

for small clusters and $\frac{1}{2}\langle 1\,1\,1\rangle$ loops are tabulated in the Supplementary Material, for the 1–100 size range.

Finally, it should be noted that in several articles the potential importance for microstructure evolution in Fe of Burgers vector flipping has been emphasised, because this type of event gives a partially 3D character to the migration of loops [149,150]; impurities may enhance this feature [151]. Unfortunately, very little if anything is known about the frequency of these events and the activation energy involved. In [10,11], following the approach devised in [6], self-interstitial clusters up to size 30 were assigned a progressively smaller probability of flipping Burgers vector and therefore 1D direction of migration. This was not done by assigning a frequency, but rather a pure probability of rotation, $e^{(-E_{rot}/k_B T)}$ [6]. In this expression, E_{rot} is a sort of "effective energy" for Burgers vector flipping. The chosen values are tabulated in the Supplementary Material.

Whenever the model distinguishes between $\frac{1}{2}\langle 1\,1\,1\rangle$ and $\langle 1\,0\,0\rangle$ loops, different mechanisms are used for the formation of $\langle 1\,0\,0\rangle$ loops. They can result from the interaction between two $\frac{1}{2}\langle 1\,1\,1\rangle$ loops [26,106,107,108] (reaction model) or nucleate from C_{15} clusters [76,106,107] (nucleation model). Self-transformation as in [103] has never been implemented in a model to our knowledge, possibly for lack of knowledge of which conditions may trigger it and thus lack of relevant parameters. The relative importance of the two mechanisms that are generally considered has been assessed in [14], concluding that the nucleation from C_{15} clusters seems to be more effective than the reaction between $\frac{1}{2}\langle 1\,1\,1\rangle$ loops to produce $\langle 1\,0\,0\rangle$ loops and obtain agreement with experimental values of loop density. However, the reference experiments were thin film ion irradiations, where the proximity of free surfaces may have biased the results, because $\frac{1}{2}\langle 1\,1\,1\rangle$ loops readily disappear there.

When applying the reaction and/or the nucleation model to create $\langle 1\,0\,0\rangle$ loops, a number of choices need to be made and parameters assigned, on which knowledge is limited or lacking, so some arbitrariness is unavoidable. In [14], following [26,108,151], the *reaction* model was applied to $\frac{1}{2}\langle 1\,1\,1\rangle$ loops above size 20 and the effect of the choice of this threshold was studied. The interaction between two $\frac{1}{2}\langle 1\,1\,1\rangle$ loops resulted in the formation of a $\langle 1\,0\,0\rangle$ loop if two conditions were simultaneously fulfilled: (1) the sum of their Burger's vectors must have a $\langle 1\,0\,0\rangle$ direction and (2) the sizes of the two interacting loops are about the same (within a 5% margin of difference, as suggested by Marian *et al.* [108,151]). If these conditions were not fulfilled, the resulting loop was simply a larger $\frac{1}{2}\langle 1\,1\,1\rangle$ loop, with the Burger's vector of the bigger one. Once the $\langle 1\,0\,0\rangle$ loops were formed, they were considered immobile and allowed to further

grow by absorbing small SIA clusters (<5 SIA) or capturing smaller $\frac{1}{2}\langle 1\,1\,1\rangle$ loops, as well as by coalescence with other loops of similar size and type. If interacting with a larger SIA loop, the final Burger's vector is always the one of the larger SIA cluster, thus $\langle 1\,0\,0\rangle$ loops may be potentially lost in this way. The *nucleation* model assumed independent creation of the two types of loops. As soon as an SIA cluster reached size 5, it may become a $\langle 1\,0\,0\rangle$ or a $\frac{1}{2}\langle 1\,1\,1\rangle$ loop according to a predefined ratio. This $\langle 1\,0\,0\rangle$ -to-$\frac{1}{2}\langle 1\,1\,1\rangle$ ratio was initially taken as 5%, following Marinica *et al.* [71], who consider this to be also the ratio of immobile C_{15} clusters formed in collision cascades, and assuming that all C_{15} clusters will grow into $\langle 1\,0\,0\rangle$ loops [106]. This ratio is, however, uncertainly known, as well as the outcome of the growth of C_{15} clusters. Recent studies suggest a ratio between 5 and 20% and more frequent transformation of C_{15} into $\frac{1}{2}\langle 1\,1\,1\rangle$ than $\langle 1\,0\,0\rangle$ loops [26,76,107], without excluding contributions from the reaction model. It is also known that $\langle 1\,0\,0\rangle$ loops become more stable as temperature increases [79]. This effect, however, has not been explicitly included so far in OKMC simulations, to our knowledge, among other reasons because this stabilising effect of temperature, which becomes the more visible the closer to the Curie temperature (1043 K = 770 °C), is likely to be experimentally indiscernible from the effect of the higher mobility of $\frac{1}{2}\langle 1\,1\,1\rangle$ loops. These will likely disappear much more efficiently at sinks, at high enough temperature, than the much more slowly migrating (or perhaps immobile) $\langle 1\,0\,0\rangle$ loops, which will be hence "left behind" and thus observed in the microscope in larger amount. The overall balance between mechanisms should eventually lead to obtain the correct $\frac{1}{2}\langle 1\,1\,1\rangle$-to-$\langle 1\,0\,0\rangle$-loop ratio, as experimentally observed, but it is easy to see that there can be many different paths and parameter choices to obtain the same result.

The above consideration on mobility and disappearance of $\frac{1}{2}\langle 1\,1\,1\rangle$ loops at sinks, leads to discussing another important point, i.e. the need to introduce traps that delay, or even completely hinder, their migration. Both models that include only one single effective type of loop (generally with properties closer to $\frac{1}{2}\langle 1\,1\,1\rangle$ than to $\langle 1\,0\,0\rangle$ loops) and models that include both will need to introduce traps of this type in order to have a chance to reproduce experimental results. Without traps, it is essentially unavoidable that all $\frac{1}{2}\langle 1\,1\,1\rangle$ loops will be lost at sinks, if they are allowed to migrate with negligible energy (<0.1 eV). There is clear experimental evidence of the existence of traps that reduce the mobility of $\frac{1}{2}\langle 1\,1\,1\rangle$ loops: Arakawa *et al.* [104] measured the diffusion coefficient of these loops, finding a migration energy of 1.3 eV, thus at least one order of magnitude larger than what simulations reveal. This has been interpreted as the result of the interaction of loops with impurities, especially interstitial solutes such as C and N, which are unavoidably present even in the purest specimen. Studies performed with interatomic potentials and DFT show that C atoms do indeed interact strongly with self-interstitial clusters and loops [152–155], as well as with vacancies [156–160]. In fact, C-vacancy complexes appear to be very efficient traps for dislocation loops [152,154], with binding energy that could explain the 1.3 eV measured by Arakawa and co-workers as effective migration energy of $\frac{1}{2}\langle 1\,1\,1\rangle$ loops [104]. These data will be discussed in the follow up papers to this work, thus here no detailed discussion is included. Simpler schemes in which trapping energy values are selected, taking inspiration from known ones for C-defect binding energy, can be found in [10] or in [14]. In the former, different trap populations were introduced, to take into account the effect of the formation of C-vacancy complexes that are also acting as traps for gliding loops [154]; in addition, traps for vacancy clusters, also inspired to C atoms, were introduced as well. The bottom line is that if a model assigns a migration energy <0.1 eV to $\frac{1}{2}\langle 1\,1\,1\rangle$ loops, then some mechanism to reduce their mobility, such as traps, needs to be introduced, otherwise in simulations at temperatures of interest for applications they will all disappear at sinks and none will remain in the volume, in clear disagreement with experimental evidence.

Binding and dissociation energy values for point-defect clusters in Fe

According to eq. (6), the dissociation energy $E_d(n)$ that is necessary for a single point-defect to be emitted from a cluster is the sum of the

Table 2a

Binding energy (E_b) of a single vacancy to a vacancy cluster as a function of cluster size in pure Fe, for the reaction $O \rightarrow O_i + O_j$, where O denotes an object that dissociates into two smaller ones, $O_{k=i,j}$.

Species	Product i	Product j	E_b (eV)	Reference
V_2	V	V	0.21	DFT [161]
			0.3	DFT [57]
			0.19	DFT [55]
V_3	V_2	V	0.36	DFT [161]
			0.37	DFT [57]
			0.46	DFT [55]
V_4	V_3	V	0.7	DFT [161]
			0.62	DFT [57]
			0.66	DFT [55]
V_5 (planar)	V_4	V	0.8	DFT [55]
V_6 (planar)	V_5	V	0.95	DFT [55]
V_7 (planar)	V_6	V	0.71	DFT [55]
V_8 (planar)	V_7	V	0.94	DFT [55]
V_9 (planar)	V_8	V	0.75	DFT [55]
V_{10} (planar)	V_9	V	0.91	DFT [55]
V_n n > 10	V_{n-1}	V	AKMC values (Suppl. Mat.); Alternatively use eqs. [15] and [16] or [17] in eq. [12]	EIP [59]

binding energy to the cluster, $E_b(n)$, which is a function of the cluster size, (once the type of cluster is defined), with the migration energy of the emitted defect, $E_{m,e}(1)$. The latter is assumed to be independent of the cluster size and to coincide with $E_m(1)$, which can be taken from Table 1a for both single self-interstitial and vacancy. The functions $E_b(n)$ are discussed in the following two sections for vacancy and self-interstitial clusters.

Vacancy clusters

Table 2a shows some of the values of binding energy obtained from DFT for single vacancies to vacancy clusters up to size 10 and indicates the values that can be used above this size.

Most data in Table 2a come from the work of Kandaskalov *et al.* [55], which is especially useful and interesting, because it extends DFT calculations to relatively large sizes, finding that planar clusters between 5 and 10 vacancies are more stable than spherical (or rather "volumetric", as they are never really spherical) ones. This result is consistent with an earlier Metropolis Monte Carlo study performed using two interatomic potentials for iron [54] and stems from the fact that small vacancy clusters can be built by adding perpendicular 2nd nearest neighbour pairs of vacancies. For sizes>10, however, volumetric clusters become again more stable than planar ones, in agreement with other DFT calculations [47,48], as well as with [54]. Fig. 4 shows the value of the

binding energy of a single vacancy to a cluster up to size 20, as calculated statically using three interatomic potentials (the configurations were selected using a Metropolis Monte Carlo method in [54]), as well as with DFT according to three different authors. This figure reveals that the results of the interatomic potentials are qualitatively, and often also quantitatively, in good agreement with DFT. In particular, the oscillating values above size 5 appear to be a constant feature, which points to the existence of cluster configurations that are inherently more stable than larger ones. The values oscillate between ~ 0.8 and ~ 1.2 eV, suggesting dissociation energy values between ~ 1.4 and ~ 1.6 eV, i.e. already activated at temperatures round 300 °C, although relatively infrequent. The good agreement between values from DFT and interatomic potentials enables the latter to be fairly reliably used to extend the set of DFT binding energy values.

Fig. 4 also includes three sets of values obtained from AKMC calculations, the same studies that provided the migration energy values in Fig. 2 [59,60]. These AKMC calculations provided *directly* the dissociation energy, from the plot versus temperature of the dissociation time, i. e. this energy was *not* calculated as the sum of migration and binding energy, as in eq. (6). On the contrary, the binding energy has been obtained in Fig. 4 by subtracting the corresponding $E_m(1)$ value from the AKMC dissociation energy. As discussed, AKMC calculations are dynamic. Thus, while their reliability is limited by the use interatomic
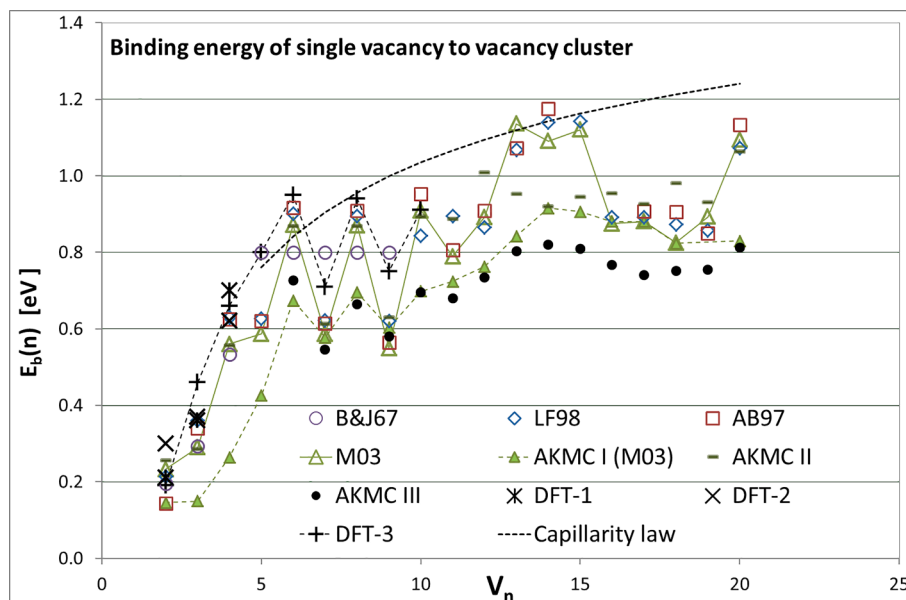

Fig. 4. Binding energy $E_b(n)$ of a single vacancy to a cluster of n vacancies up to size 20, as obtained from a Metropolis Monte Carlo study using interatomic potentials: LF98 [162], AB97 [163] and M03 [146]. The data points denoted as B&J67 are taken from a very early computational work by Beeler and Johnson, where a pair potential was used [164]. The data points denoted as AKMC I (M03) [59], AKMC II and AKMC III [60] come from the same work as in Fig. 2, see corresponding text. The three DFT data sets come from, respectively, [161]-1, [57]-2, and [55]-3. The smooth dotted line corresponds to applying the capillarity law (eq. (15)), with $E_b(2) = 0.2$ eV and $E_f(1) = 2$ eV, which provides a sort of upper bound.

potentials and/or by the hypothesis made for energy calculation when fitted to DFT, the way the dissociation energy is obtained inherently allows for the continuous reconfiguration of the cluster while vacancies are moving. This is important because the emission of a point-defect is more likely to occur when the cluster is in a configuration that is *not* the most stable one, i.e. when the actual binding energy is temporarily lower. It is therefore expected that the dissociation energy obtained by AKMC calculation should be *lower* than the one stemming from static calculations, which implicitly assume that defect emission occurs starting from the most stable cluster configuration. Consistently, the data points from the most complete AKMC study [59] in Fig. 4 are significantly lower than the static ones (even those obtained from the same potential, M03). The other two AKMC studies, II and III, globally also follow the same trend, in particular AKMC III values are almost identical to AKMC I values, despite the very different way in which they were parameterised. AKMC II by chance provides for small clusters values that are identical to those obtained statically with M03. The complete tabulation of the AKMC I data is given in the Supplementary Material and is here recommended as parameter set to be used.

The AKMC I calculations have been extended up to clusters of 250 vacancies. In order to extrapolate beyond this size it is necessary to use appropriate equations. One that is often used to calculate the binding energy of a defect from a defect cluster, starting from vacancy n > 4, is the capillary law [165]:

$$E_b(n) = E_f(1) - \frac{(n^{\frac{2}{3}} - (n-1)^{\frac{2}{3}})(E_f(1) - E_b(2))}{2^{\frac{2}{3}} - 1} \quad (15)$$

Here $E_f(1)$ is the formation energy of the single point-defect. According to DFT the formation energy of a vacancy varies between 1.95 and 2.15 eV, while the experimental values are lower and can vary between 1.5 and 2.0 eV [58]. The fact that experiments provide lower values may be due to the entropic effect at the high temperature that is needed to have a sufficiently high concentration of vacancies and allow their detection (see detailed description of the kind of experiment performed - although the conclusions of the work are wrong - in [166], to be combined with the vacancy formation entropy calculations in [167]). $E_b(2)$, the binding energy of a pair of point-defects, can be taken from Table 2a. In practice, two fair values for these parameters are:

$$E_b(2) = 0.2 \text{ eV}$$

$$E_f(1) = 2 \text{ eV} \quad (16)$$

The $E_b(n)$ function from eq. (15) with the above parameter values is shown in Fig. 4: opposite to the AKMC values, it provides a sort of upper bound, without of course reproducing any of the oscillations. The $E_b(n)$ function can also be obtained from eq. (12), provided that a derivable expression for the formation energy versus size, $E_f(n)$, is available. In [47] the following equation is proposed:

$$E_f(n) = 4\pi\sigma\left(\frac{3n\Omega}{4\pi}\right)^{2/3} \quad (17)$$

where $\Omega = a_0^3/2 = 11.82 \text{ Å}^3$ is the formation volume of a vacancy in iron, $a = 2.87 \text{ Å}$ being the lattice constant, and $\sigma = 1.7 \text{ J/m}^2$ is the average surface energy.

Fig. 5 compares the $E_b(n)$ values obtained from eq (15) – capillary law - and from the generic expression of eq. (12), with $E_b(2)$ and $E_f(1)$ as in eq. (16) and using eq. (17) to derive the formation energy $E_f(n)$ in eq. (12). In the same figure, the AKMC I binding energy curve is plotted up to $n = 200$. Again, the AKMC calculation predicts significantly lower values for dissociation than any equation and this happens because the AKMC simulations implicitly take into account the fact that dissociation occurs from configurations that are not the most stable ones, which temporarily created and correspond to the easiest starting point for vacancy emission. Thus neither analytical expression seems especially suitable to extrapolate the AKMC values, unless the $E_f(1)$ and $E_b(2)$
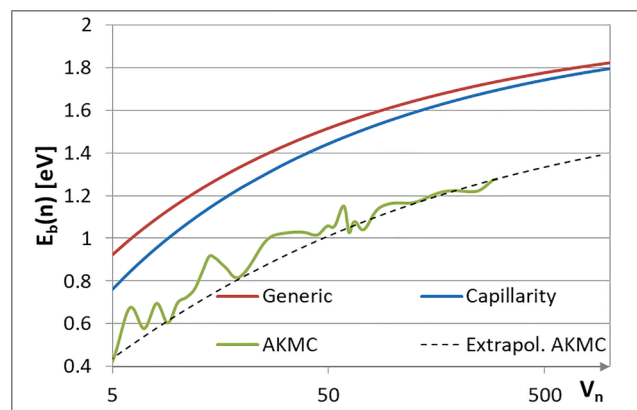

Fig. 5. Binding energy $E_b(n)$ of a single vacancy to a vacancy cluster of size n up to 1000, obtained from different expressions: (a) the generic expression of eq. (12), using eq. (17) to express the cluster formation energy $E_f(n)$ and with $E_f(1) = 2$ eV; (b) the capillary law, eq. (15), with $E_b(2) = 0.2$ eV and $E_f(1) = 2$ eV; (c) the dissociation energy results from AKMC [59] after subtracting the single-vacancy migration energy, $E_m(1) = 0.63$ eV; (d) its extrapolation to large sizes as in eq. (18).

values are suitably fitted. The AKMC curve also reveals that oscillations continue to appear at irregular periods for sizes above $n = 20$, as well; these oscillations should be ascribed to the existence of sort of "magic numbers" that correspond to especially stable configurations: even though most likely not all of these "magic numbers" have been identified by the AKMC study, and they likely depend on the choice of the approximations that are inherent to the specific AKMC model, in principle the oscillations should be considered to have a physical origin. Thus the $E_b(n)$ function is not a monotonically growing one, at least not for small-to-medium cavity sizes, and therefore strictly speaking the use of simple power functions, such as eq. (15) or eq. (12) with eq. (17), is not fully correct. However, extrapolation is necessary and it is here argued that it is best to extrapolate the AKMC data themselves beyond $n = 250$. The following expression provides a smooth extrapolation:

$$E_b(n) = 1.71 - 2.76[(n+1)^{0.73} - n^{0.73}] \quad (18)$$

Here, 1.71 eV is the formation energy of the vacancy according to the interatomic potential used for the AKMC calculations, so this equation is formally of the same type as eq. (12). The corresponding curve is also shown in Fig. 5.

Self-interstitial clusters

Table 2b lists the DFT values for the binding energy as a function of n in the case of small self-interstitial clusters. It is clear that the binding energy in this case grows faster than for vacancies, being as high as 1.6 eV already for the tri-interstitial, according to DFT, which implies a dissociation energy close to 2 eV. Therefore, except for the very small clusters (2–3 SIAs), it is legitimate to consider that this dissociation is forbidden.

Table 2b
Binding energy (E_b) of a single self-interstitial to a cluster in pure α-Fe.

Species	Product i	Product j	E_b (eV)	Reference
I ⟨110⟩ 2	I	I	0.8	DFT [57]
I ⟨110⟩ 3	I2	I	0.92	DFT [57]
I ⟨110⟩ 4	I3	I	1.64	DFT [57]
			0.96	[12]
In ⟨100⟩ or ½⟨111⟩>4	In-1	I	Any equation as in Fig. 6 or series of discrete values	E.g. [57]
			Or dissociation forbidden	E.g. [10]

Table 2c
Coefficients c_i for the application of eq. (19).

Type of loop ↓ / c_i (eV) →	c_0	c_1	c_2
½⟨111⟩	1.60485	5.35226	−0.147319
⟨100⟩	1.77677	7.15951	−5.81801

As an alternative, for simulations at relatively high temperature, where thermal dissociation of (small) self-interstitial clusters may be activated, an equation is needed. Eq. (15) was used in [57]. The value of $E_f(1)$ for the self-interstitial atom in Fe varies between 3.64 and 4.0 eV according to DFT calculations, while experimental estimates are higher and close to 5 eV [58]. $E_b(2)$ can be taken from Table 2b (0.8 eV). However, strictly speaking the application of Eq. (15) is not totally legitimate for self-interstitial clusters, because it implicitly assumes a cluster with spherical shape (similarly to eq. (17)). It is therefore more physical to apply the generic eq. (12), using for example the following expression for $E_f(n)$ [80]:

$$E_f(n) = c_0 \sqrt{n} ln n + c_1 \sqrt{n} + c_2 \qquad (19)$$

This equation gives the formation energy of a loop of n defects. The values of the coefficients depend on the loop Burgers vector, as in Table 2c.

Fig. 6 shows the curves $E_b(n)$ obtained: (1) by applying eq. (15) to self-interstitial clusters (with $E_f(1) = 3.64$ eV and $E_b(2) = 0.80$); (2) by using eq. (19) to feed eq. (12) (for both ½⟨111⟩ and ⟨100⟩ loops), also with $E_f(1) = 3.64$. For comparison, the curves for vacancies of Fig. 4 are shown in Fig. 5, as well. It can be seen that the binding energy of self-interstitials to loops predicted by these equations is about twice as high as for vacancies, at equal size. The capillarity law gives the highest binding, while the binding to ½⟨111⟩ loops is stronger than to ⟨100⟩ loops, consistently with their stability that goes in the opposite order. Focusing on the small sizes, the curve obtained from the formation energy of ⟨100⟩ loops is the only one that predicts, for sizes 5 and 6, a lower binding energy for self-interstitials than for vacancies, at odds with DFT calculations, that suggest a value of binding energy of 0.8 eV already for the di-interstitial (which corresponds to a dissociation energy of 1.1 eV). Thus, except if demonstrated that the binding energy for clusters with 4 to 6 self-interstitials is actually lower than for di- or tri-interstitial, which seems unlikely, none of the curves can be used to extrapolate smoothly from the DFT data of Table 2b, with $E_f(1) = 3.64$. $E_f(1)$ needs to be increased beyond its DFT upper limit of 4 eV in order to extrapolate (with the ⟨100⟩ loop curve) the (non-DFT) value of 0.96 eV for the tetra-interstitial from Table 2b, and needs to be increased beyond

5 eV to intercept the DFT value of 1.64 eV. By doing so, all curves are shifted upward, providing dissociation energy values in excess of 2 eV even for clusters of 5–6 SIAs. Events of this type become activated only beyond 400 °C. In general, assuming no dissociation for self-interstitial clusters is therefore an acceptable approximation, except perhaps in the case of di- and tri-interstitial, the dissociation of which, however, has about the same activation energy as the migration of a large void and is therefore very unlikely.

Attempt frequencies for point-defect clusters in Fe

Attempt frequency for migration

Eqs. (2), (5), (7), (8) show that the attempt frequency (or prefactor) needs to be known to obtain the diffusion coefficient of the defects. As a standard, the attempt frequency for single-point defect migration, henceforth denoted as $\nu_m(1)$, which corresponds to the vibration frequency in the direction of the reaction path [110], is expected to be close to the vibrational frequency of the lattice (Debye frequency), which for iron is about $6.1 \cdot 10^{13}$ s^{-1}.[2] However, different values for $\nu_m(1)$ have been used by different authors, in a range between an order of magnitude smaller or bigger than the mentioned value, as exemplified in Table 3a. Except when stemming from MD calculations, no justification is generally given for the choice, but it is also implicitly assumed that the actual choice of the value of the point-defect attempt frequency is not overwhelmingly important, although to our knowledge no study has been performed on this issue. DFT calculations for single point-defects also exist [168,169], which have been included in Table 3a.

Like most other parameters, the prefactor of the diffusion coefficient of a cluster depends on its size, type and configuration, which influence both dimensionality and mechanisms of diffusion. As mentioned, the dimensionality and also the inherent mechanism of diffusion are very different in the case of vacancy and self-interstitial clusters; they also vary depending on the configuration of the self-interstitial cluster.

For 3D migrating vacancy clusters, a thorough study of attempt frequencies was performed using AKMC calculations [59], which provided values for the attempt frequencies for both migration and dissociation (see section 3.3.2 for the latter), up to size 250. These values are shown in Fig. 7 in terms of ratios $\nu_m(n)/\nu_m(1)$: the figure shows the AKMC I values [59], together with the more limited AKMC II and III data [60]. It can be seen that, depending on the model, the values can vary by a couple of orders of magnitude, but only for relatively few clusters. The agreement between models is less satisfactory than in the case of the
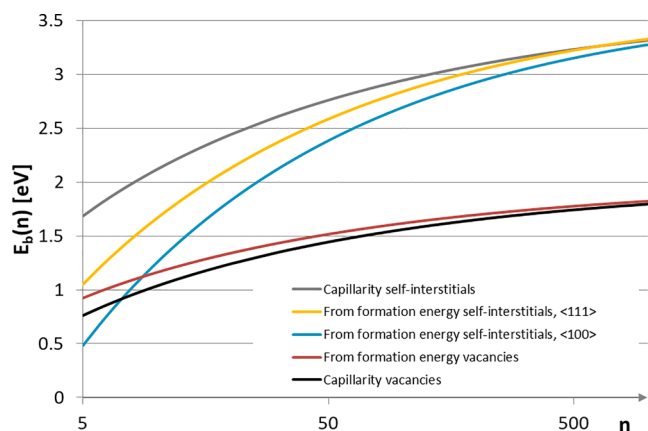

Fig. 6. Binding energy $E_b(n)$ of a single self-interstitial to a self-interstitial cluster of size n up to size 1000, obtained from eq. (12), or by combining eq. (16) and eq. (10), with $E_b(2) = 0.8$ eV and $E_f(1) = 3.64$ eV. For comparison the same curves as in Fig. 3, for vacancies, are also plotted.

Table 3a
Attempt frequencies for single point-defects, $\nu_m(1)$, and corresponding diffusion coefficient prefactor, D_0, as chosen in the cited articles (except for DFT, the calculation method is not specified as it is not always given in the reference and it may be just a "reasonable choice").

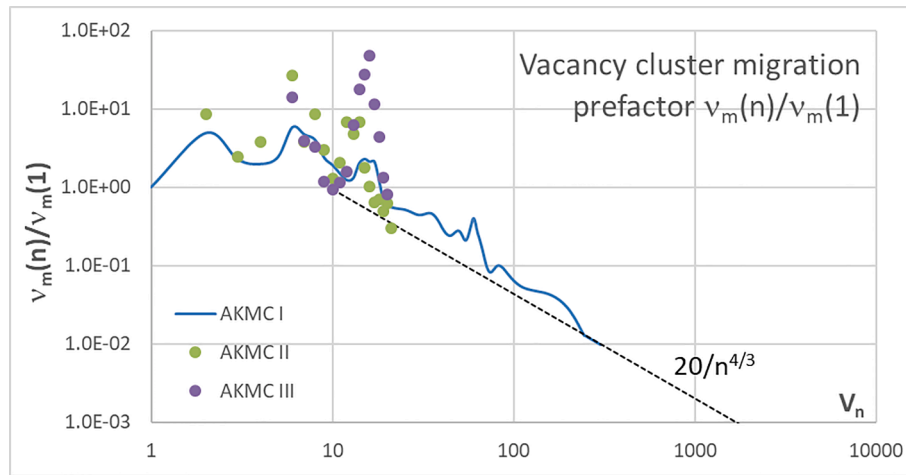| Species (V = vacancy, I = self-interstitial)	Reference	$\nu_m(1)$ (10^{13}s^{-1})	$D_0(1)$ (10^{-8} m^{2}s^{-1})
V	DFT [168]]	11.6	116
	[2–5]	1.12	115.0
I	DFT [169]	0.44	37.5
	[2–5]	2.04	20.9
V/I	[6,10,11,15–23]	0.6	6.15
V/I and all defects	[7]	0.1	1.03
V/I and all defects	[8]	8.0	82.0
V/I	[14]	13.4	137
V	Recommended	1.0	10.25
I	Recommended	8.07	83.1

Fig. 7. Attempt frequency for vacancy cluster migration $\nu_m(n)$, normalised over $\nu_m(1)$, versus cluster size as obtained from AKMC simulations [59,60] and function used to extrapolate to any size according to eq. (20).

migration energy (Fig. 2), although the peaks are roughly in agreement.

For clusters of n > 250 vacancies, the attempt frequency for migration as a function of size, $\nu_m(n)$, can be extrapolated using the following equation:

$$\frac{\nu_m(n)}{\nu_m(1)} \simeq \frac{a}{n^{\frac{4}{3}}} \tag{20}$$

where a is a constant that has to be determined in order to smoothly extrapolate from smaller clusters' values. Eq. (20) originates from the idea of vacancy migration along the internal surface of the void [170]: for a heuristic demonstration see Appendix A.1. In order to extrapolate correctly from other data, a constant value may need to be added. In Fig. 7 the AKMC I data points are joined with eq. (20) by setting $a = 20.0$. The Supplementary Material provides the full tabulation of the data points of Fig. 5 up to size 300. We recommend the use of the tabulated values and their further extrapolation according to eq. (20).

For small self-interstitial clusters (up to size 7), MD simulations with an interatomic potential have provided fairly reliable values [64], even though they do not allow for the formation of non-parallel configurations (C_{15}). These are listed in Table 3b.

For self-interstitial clusters of type ½⟨111⟩ and large size, a prefactor obtained from early MD simulations [3] can be used [3–5]:

$$\nu_m(n) = 3.4\hat{A}\cdot10^{12} + \frac{1.65\hat{A}\cdot10^{13}}{n^{1.7}} \tag{21}$$

Using this expression, however, the attempt frequency becomes quickly a constant, equal to $3.4\cdot10^{12}$ s^{-1}, because of the high exponent of n. Therefore, in practice most clusters will migrate with this attempt frequency, without any size dependence.

Alternatively, in [10,11,15–23] a different scaling law was used for the migration of self-interstitial clusters with n > 7, namely:

$$\nu_m(n) \simeq \frac{b}{n^{0.8}} \tag{22}$$

The value 0.8 as exponent of n in the denominator has been determined experimentally by Arakawa and co-workers [104]. This exponent complies with the theory, given that it should theoretically lie between the two limiting cases 0.5 and 1: the former corresponds to migration purely via independent crowdion model [85], the second one to migration via kink pair formation along the edge of the loop [81]. The intermediate value of 0.8 suggests a mixture between these two mechanisms. MD simulations have confirmed similar trends, with coefficients that vary between 0.5 and 0.85 [63]. In order to use eq. (22) to extrapolate smoothly from the values of Table 3b, one can choose for example $b = 8.11\cdot10^{12}$ s^{-1}. In the case of large clusters, the attempt frequency obtained using eq. (22) can be more than one order of magnitude smaller than using eq. (21), thereby predicting a significantly slower mobility of large loops. Fig. 8 shows the prefactor for self-interstitial cluster migration, normalised to the prefactor of the single interstitial (Table 3b), $\nu_m(1)$, as a function of size, joining eq. (22) with the values of Table 3b, which is the combination that we recommend, and compares it to eq. (21).
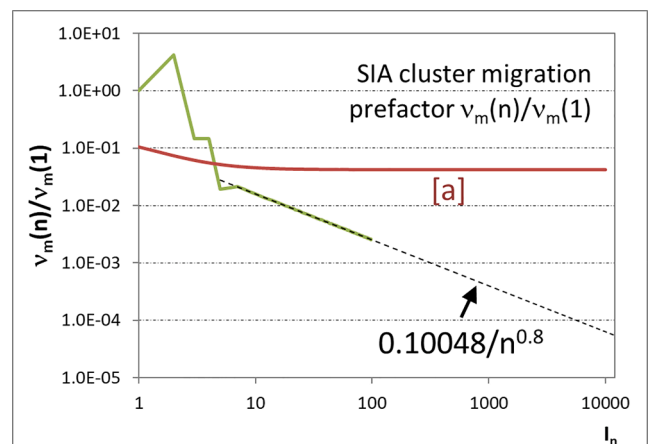
Table 3b
Attempt frequencies, $\nu_m(n)$, and corresponding diffusion coefficient prefactor, D_0, for small self-interstitial clusters in pure Fe, as calculated in [64].

Species	Migration type	$\nu_m(n)$ (10^{13}s^{-1})	$D_0(n)$ (10^{-8} m^{2}s^{-1})
I ⟨110⟩	3D	8.07	83.1
I ⟨110⟩ 2	3D	34.15	351
I ⟨110⟩ 3	3D/1D	1.18	12.1
I ⟨110⟩ 4	3D/1D	1.20	12.3
I ⟨111⟩ 5	1D	0.16*	1.56*
I ⟨111⟩ 7	1D	0.17	1.71
*Used also for size 6			

Fig. 8. Attempt frequency for SIA cluster migration $\nu_m(n)$, normalised over $\nu_m(1)$, versus cluster size as obtained from MD simulations [64] and function used to extrapolate to any size according to eq. (22), as well as to eq. (21), the latter denoted as [a].
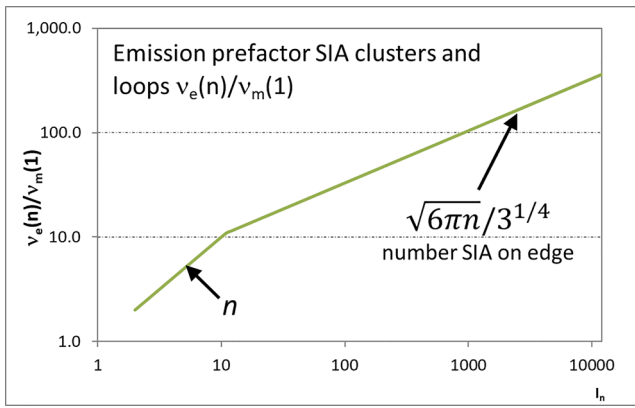
Fig. 9. Attempt frequency for single SIA emission from a loop, $\nu_e(n)$, normalised over $\nu_m(1)$, versus cluster size: note the switch from direct proportionality with size to proportionality with the number of peripheral SIAs at size 10.

Attempt frequency for dissociation

We assume here that only one point-defect at a time is emitted from a cluster, so the dissociation frequency might a priori be considered equal to $\nu_m(1)$. Intuitively, however, the prefactor for emission, which embodies the rate at which one point-defect makes an *attempt* to be emitted, should depend on the size n of the cluster, because the more point defects, the more likely that one of them *tries* to jump away. In some OKMC codes, for example MMonCa [9,12,14], every defect in a cluster is individually defined. In this case, the solution that is naturally applied corresponds to assuming that:

$$v_e(n) = n v_m(1) \tag{23}$$

This approximation is likely to be fairly correct for small point-defect clusters, which do not have a well-defined interface with the rest of the crystal. This is especially true for self-interstitial clusters, which do not have a volumetric configuration and can only emit when they are very small (2–3 SIAs). This is, however, an overestimation of the dissociation rate for the case of large clusters, since eq. (23) assumes that all point-defects in the cluster are equally likely to dissociate, which is clearly not true when only the point-defect located at the cluster periphery can in fact be emitted. The dissociation of self-interstitials from loops is effectively very unlikely, because of the high binding energy. However, if one wants to describe this dissociation process it seems intuitive to

introduce a dependence on the number of self-interstitials located on the loop edge, such as:

$$\frac{v_e(n)}{v_m(1)} = \sqrt{6\pi n}/3^{1/4} \tag{24}$$

Here, the right hand side is an estimation that can be obtained after attributing a circular shape to a hexagonal loop, having in mind $\frac{1}{2}\langle 1\,1\,1\rangle$ loops. The switch between eqs. (23) and (24) occurs at $n = 10$, which is a reasonable size. This can be seen in Fig. 9.

Similarly, in the case of sufficiently large vacancy clusters, one may think of considering the pre-factor for emission to be proprotional to the surface of the spherical cavity. However, in order to be consistent with the rate theory and guarantee that absorption and emission of single defects can reach steady state kinetic equilibrium, the vacancy emission rate must in fact be proportional to the radius of the cavity (assumed to be spherical), rather than to its surface [13]. Thus, $v_e(n)$ must scale as the power $^1/_3$ of the number of vacancies, n; specifically, it can be shown (see Appendix A.2 for a heuristic demonstration) that:

$$\frac{\nu_e(n)}{\nu_m(1)} \simeq 1.5 n^{\frac{1}{3}} \tag{25}$$

This equation provides the scaling of $\nu_e(n)$ in the limit of large vacancy clusters, or anyway defects that tend to have a spherical shape. Note that an equivalent calculation based on the equivalence of absorbed and emitted self-interstitial atoms from a self-interstitial loop should be done, as well, i.e. eq. (24) is actually not correct. However, given the unlikeliness of self-interstitial emission from loops, it is here assumed that the use of eqs. (23) and (24) with switch at n = 10 as in Fig. 9 is a sufficiently good approximation. For vacancy clusters of small and intermediate sizes, AKMC simulations have provided the emission attempt frequency, in terms of ratio $\nu_e(n)/\nu_m(1)$, up to n = 250 [59]. Above this size, a function like eq. (22) has been fitted to extrapolate from the AKMC results, finding:

$$\frac{\nu_e(n)}{\nu_m(1)} = 15.84 n^{\frac{1}{3}} \tag{26}$$

Fig. 10 shows the curve of this ratio as a function of size for vacancy clusters, joining the AKMC I values from [59] with eq. (23). The full tabulation up to size 300 is given in the Supplementary Material. In this case the data points obtained with other AKMC models denote that the dispersion can be significant and the actual attempt frequency may vary by a couple of orders of magnitudes, depending on the model used.
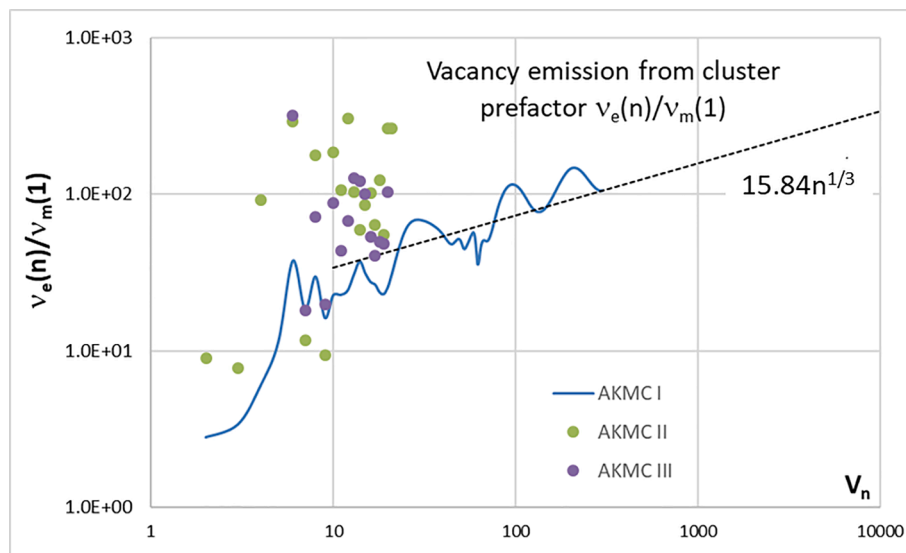

Fig. 10. Attempt frequency for vacancy emission from a cluster, $\nu_e(n)$, normalised over $\nu_m(1)$, versus cluster size as obtained from AKMC simulations [59,60] and function used to extrapolate to any size according to eq. (26).
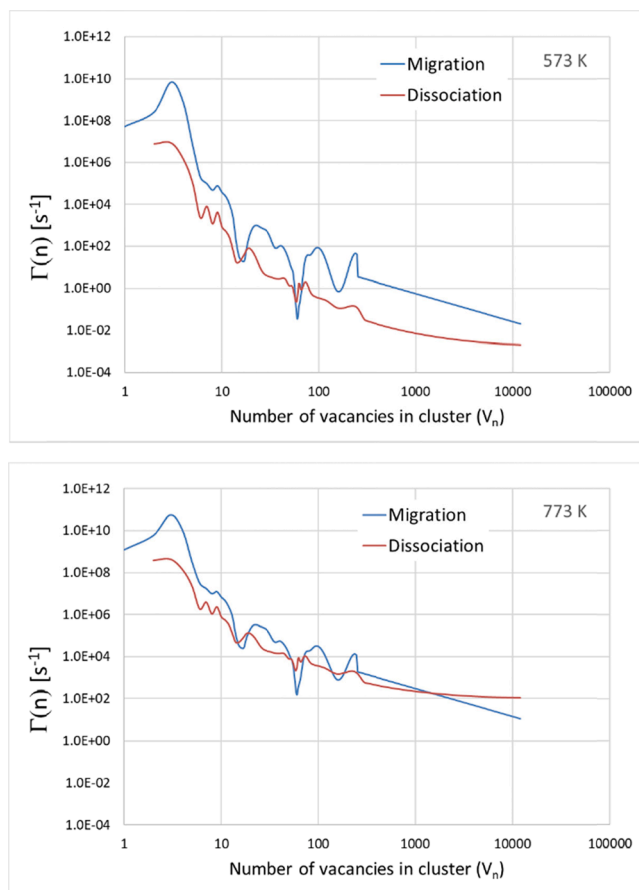
Fig. 11. The frequency of migration (jump) and dissociation (emission of a vacancy) as functions of vacancy cluster size at 573 K (left) and at 773 K (right). The attempt frequency of the single vacancy, $\nu_m(1)$, has been chosen equal to $1 \cdot 10^{13}$ s^{-1} (Table 3a).

Migration versus emission frequency: Thermal stability of point-defect clusters

When used to calculate the frequency of key events, such as migration and dissociation of clusters, the set of parameters presented above quantitatively accounts for effects that, although qualitatively known, are useful to be looked into in some detail, to get an idea of the orders of magnitude involved.

Fig. 11 compares the frequency of migration of vacancy clusters with the frequency of dissociation by emission of a vacancy at 300 and 500 °C, as functions of size.

It emerges clearly that at 300 °C only clusters of less than 15 vacancies will jump more than once per ms, some of them with very high frequency (the tri-vacancy will jump about 100 million times per ms), but most of them with rapidly decreasing frequency with increasing size. For essentially all sizes migration is significantly more frequent than emission. At 500 °C, in contrast, even clusters of more than100 vacancies may migrate with frequencies higher than once per ms, i.e. rapid and efficient migration of sizeable cavities becomes possible at this temperature. Migration enhances the possibility that clusters coalesce and thus helps the formation of large voids which, the larger, the less likely to emit and shrink (as well as to migrate). Thus void will tend to be larger and present in maller densitiy at higher temperature. However, the temperature increase affects more the dissociation than the migration. Namely, at 500 °C emission and migration have comparable frequency in many size ranges and large cavities are more likely to
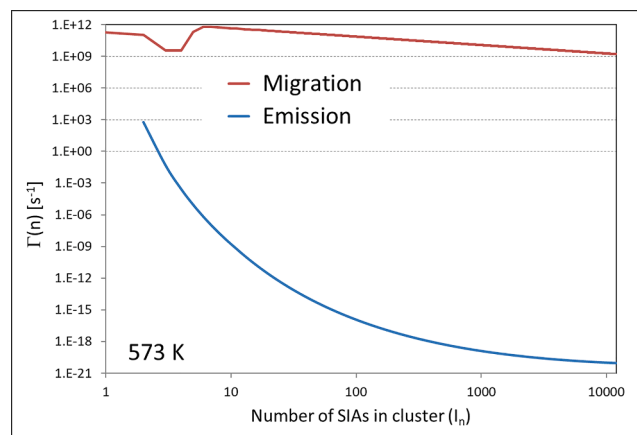

Fig. 12. Frequency of migration (jump) and dissociation (emission of a self-interstitial) as a function of self-interstitial cluster size at 573 K. The attempt frequency of the single self-interstitial, $\nu_m(1)$, has been chosen equal to $8.07 \cdot 10^{13}$ s^{-1} (Tables 3a and 3b).

dissociate than to migrate (the cross-over occurs for voids of about 1300 vacancies). This corresponds to the widespread notion that vacancy clusters are thermally unstable and voids will dissolve at sufficiently high temperature. Interestingly, because of the jagged shape of the curves, there are some clusters that, because of their size, will rather emit than jump even at 300 °C. Even though it is far fetched to expect that this effect will have any significant impact on the microstructure evolution, as is to believe that the parameters used here correctly catch all the cases of this type, the use of monotonically growing curves for the migration and binding energy would never reproduce this feature.

The situation is significantly different in the case of self-interstitial clusters. Their migration energy is lower than in the case of vacancy clusters: self-interstitial loops migrate with energy an order of magnitude lower than sizeable voids. On the other hand, as shown in Fig. 6, the energy for emission is about a factor two higher in the case of self-interstitial clusters than vacancy clusters, for all sizes. As a consequence, these clusters will only migrate, with frequencies always higher than 10 million times per ms even for large sizes (except if trapped of course), and will basically never dissociate, as can be seen in Fig. 12 for the case of 300 °C. Increasing the temperature to 500 °C will not
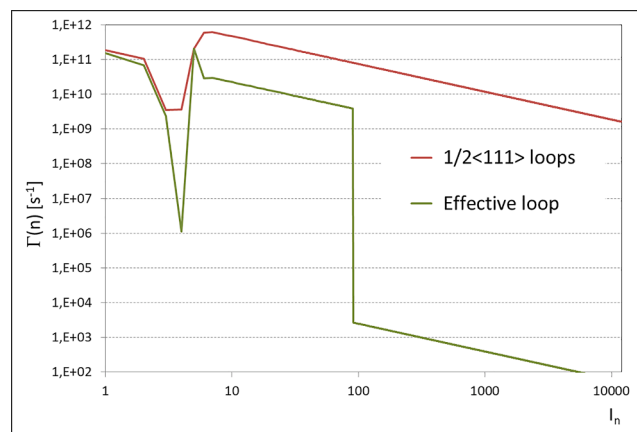

Fig. 13. Jump frequency versus SIA cluster size, Γ(n), at 300 °C, using the migration energy choice made in this work, which applies to glissile ½⟨111⟩ loops, and as in [10], where effective values without loop Burgers vector distinction were used (effective loop).

qualitatively change the situation, therefore these clusters, besides absorbing vacancies, will disappear by absorption at sinks or coalescing until forming dislocation networks, but will not dissolve under any circumstance. On the other hand, the lack of detailed information about the effective migration energy of the self-interstitial clusters, especially the small ones, and the type of choice that is made to describe loops (one generic type as in [10,11,15–23] or distinguishing between ½⟨1 1 1⟩ and ⟨1 0 0⟩) leads to jagged jump frequency curves that may differ very significantly from each other, by several orders of magnitudes, as can be seen in Fig. 13, with unavoidably strong impacts on the results of the corresponding model. This clearly shows that our current knowledge on the migration of self-interstitial clusters, due to their different possible configurations, remains fairly rudimentary: more work would be needed to not only understand the physics, but importantly to produce reliable numbers that can be used with confidence in microstructure evolution models.

Capture radii

The definition and thus also the value used for the capture radii can vary significantly from one model and one code to another. In some cases, each defect has an associated radius that depends only on its type and size and defines a spherical volume around it. Other geometries can also be considered, as is explained below. In this scheme (henceforth *Scheme A*), two objects interact when the volumes around each of them overlap [6,10,11,15–23]. In other models, the capture radius, perhaps in this case better denoted as capture distance, is a function of the two objects involved and interaction occurs when the distance between the two is smaller than the established threshold distance [2–5,8,9,13,14] (*Scheme B*). A special case of Scheme B corresponds to models where the interaction is assumed to occur between single point-defects located in two different clusters. In this third scheme the capture distance does not depend explicitly on size: this is done e.g. in [9,14]. Fig. 14 illustrates
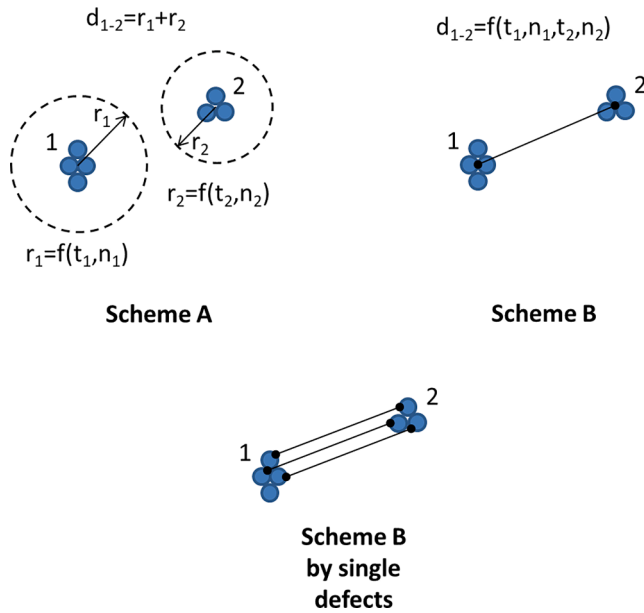

Fig. 14. Illustration of the schemes generally used in OKMC models to define the distance at which two objects interact, leading to clustering or recombination (but also trapping or absorption if one of the objects is a sink). Scheme A associates a volume with each defect that only depends on the features of that defect: interaction occurs when two volumes overlap. Scheme B defines the distance of interaction based on the features of both defects and is therefore more general than Scheme A: any Scheme A can always be expressed as a Scheme B, but not necessarily vice versa. A special case of Scheme B corresponds to checking the interaction between single point defects located in different clusters.

the different schemes. Biases can be introduced by giving a larger capture radius for interactions involving self-interstitials than for interactions involving vacancies. Whichever the criterion, capture radii definitions are always affected by a dose of arbitrariness.

One crucial piece of information that is needed in order to define the scaling of the capture radius for recombination is the distance at which a vacancy and a self-interstitial (a Frenkel pair) recombine spontaneously, R_{FP}. Experimentally, this recombination distance is reported to vary between 2.2 and 3.3 times the lattice parameter, a_0, corresponding to 100–300 atomic volumes in spherical approximation [171,172]. Choices of this order are generally made in rate theory models [165,173]. Early MD simulations with empirical potentials predicted smaller distances: $1.7a_0$ [174] or $1.9a_0$ [1]. Recently, Nakashima *et al.* [175] have determined R_{FP} using the SEAKMC method [24–26] and have obtained a value of $2.26a_0$. This value seems to be the intersection between experimental uncertainty and computational variability. Notwithstanding, in [10,11] the choice $R_{FP} = 3.3a_0$ as in [172] provided very reasonable results. The value that is chosen for R_{FP} is important because any expression used for the capture radius of defects as function of their size needs to yield this value when applied to Frenkel pair recombination, therefore it can be used to fit parameters that appear in the capture radius expression. Nakashima *et al.* [173] also calculated the interaction distance between a void and a self-interstitial atom, obtaining the following law:

$$R_{int-void/SIA} = \alpha n^{\frac{1}{3}} + \delta \tag{27}$$

where n is the number of vacancies in the void, $\alpha = 0.86a_0$ and $\delta = 1.41a_0$.

As an example of Scheme A, in [6] the capture radii were defined as follows:

$$r_i(n) = \gamma_i \left[(r_0 + \varepsilon) + a_0 \left(\frac{3}{8\pi} \right)^{\frac{1}{3}} (n^{\frac{1}{3}} - 1) \right] \tag{28}$$

In this equation: the subscript i indicates the type of defects in the cluster, vacancies ($i = V$) or self-interstitials ($i = I$); γ_i is the bias and equals 1 in the case of vacancies ($\gamma_V = 1$), while it is >1 in the case of self-interstitials (e.g. $\gamma_I = 1.15$ or 1.2); ε is a small positive quantity that is used to avoid numerical round off problems; r_0 is a fixed distance that is fitted by imposing that the Frenkel pair recombination distance should take a given value, for example $3.3a_0$ [10,11].

The idea behind eq. (28) is that a spherical shape is associated with any point-defect cluster. Its volume is estimated as a function of the number of defects n, assuming they fill a sphere. Namely, if r is the radius of the sphere, then

$$\frac{4\pi}{3} r^3 = n \frac{a_0^3}{2} \rightarrow r(n) = a_0 \left(\frac{3n}{8\pi} \right)^{\frac{1}{3}} \tag{29}$$

where $a_0^3/2$ is the atomic volume in the bcc lattice. An extra spherical shell is then added, which accounts for the extension of the strain field around the cluster (after removing the volume of the outer defects in the cluster, which is otherwise counted twice). Thus each cluster migrates taking with it a spherical volume that strictly depends only on the size and type (through the bias) of the cluster itself, while is independent of the cluster with which it interacts. Interaction occurs, as mentioned, when two volumes overlap, i.e. when the distance between the centre of mass of the two clusters is less than the sum of the two capture radii (Fig. 14).

In [10,11], eq. (28) was used only for vacancy clusters. In the case of self-interstitial clusters, it was replaced by the following expression:

$$r_I(n) = r_{0,I} + \frac{a_0}{\sqrt{\pi\sqrt{3}}} \left(\sqrt{n} - 1 \right) \tag{30}$$

with $r_{0,I} = \gamma \frac{R_{FP}}{1+\gamma} + \varepsilon$ ($\gamma = 1.2$ [10,11]).

Table 4
Comparison of the loop radius obtained from eq. (30), with $R_{FP} = 3.3a_0$, to characteristic distances obtained from atomistic studies of loop strain fields [176,177].

n	$r_I(n)$ eq. (30)	Radius at pressure peak	Radius at zero pressure	Distance at which the strain field vanishes normal to habit plane	Distance at which hydrostatic pressure vanishes normal to habit plane	Distance at which there is zero interaction with point-defect normal to habit plane	Reference
	nm						
½⟨111⟩ loops							
19	0.93	1	1.5	4.5	4.5		[176]
91	1.57					2.5–3.0	[177]
127	1.78	1.75	3	10	8.0		[176]
331	2.63	2.5	3.7	2.5–3.7			[177]
469	3.06	3	5.25	>15	>20		[176]
⟨100⟩ loops							
122	1.75					2.0–2.3	[177]
442	2.98	2.9		2.9–4.3			[177]

Using similar notation for consistency, the capture radius for vacancy clusters can be written as

$$r_V(n) = r_{0,V} + a_0 \left(\frac{3}{8\pi}\right)^{\frac{1}{3}} (n^{\frac{1}{3}} - 1) \qquad (31)$$

where $r_{0,V} = \frac{R_{FP}}{1+\gamma} + \varepsilon$. This equation is identical to eq. (28) applied to vacancy clusters.

The logic in eq. (30) is that in a self-interstitial cluster with the shape of a loop, the defects are not distributed in a sphere, but on a disc. Thus the radius of the sphere associated with the loop is equalled to the radius of the disc, where by radius of the disc we mean the actual radius (size) of the loop.

The radius (in the sense of size, not capture radius) of a perfect, hexagonal ½⟨111⟩ loop can be calculated in two different ways, as is explained in Appendix A3, leading to the following two expressions:
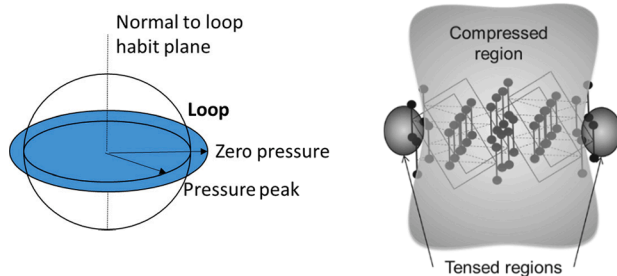
$$r_I(n) \cong 0.299 a_0 n^{0.57} \qquad (32)$$

$$r_I(n) = a_0 \sqrt{\frac{n}{\pi\sqrt{3}}} \cong 0.429 a_0 n^{0.5} \qquad (33)$$

The latter has been used to obtain eq. (30). Eqs. (32) and (33) give obviously different numerical values, but are overall very similar: the former yields slightly smaller values for small loops, but somewhat larger values for larger ones, because of the slightly larger exponent in the power law.

In order to have an idea of what the radius from eq. (30) may represent physically, Table 4 compares with it a few distances from loop strain field atomistic calculations.

The values in Table 4 suggest that the radius obtained from eq. (30) (with $R_{FP} = 3.3a_0$) gives a reasonable estimate of the radius of peak pressure, thus in this respect it is smaller than the extension of the strain field in the radial direction. The table also reveals that, despite variability between studies, most likely stemming from the interatomic potential used, as well as on the criterion used (vanishing pressure, vanishing strain, vanishing interaction with point-defects, …), the extension of the strain field in the direction normal to the centre of the loop, along the direction that crosses the centre of the loop, is even more strongly underestimated by the radius given by eq. (30), by a factor between 1.5 and 5. The situation is pictorially illustrated in Fig. 15.

Despite its obvious limitations, eq. (30) enabled very reasonable results to be obtained in comparison with experiments in [10,11] (setting $R_{FP} = 3.3a_0$); the same results could not be obtained using eq. (28) applied to self-interstitial clusters [10,11]. Moreover, the distance at which a single SIA spontaneously joins a loop when approaching it along the radial distance on the habit plane has been calculated for perfect loops from 61 to 331, by means of molecular statics techniques by one of the authors (Anento, N., details to be published), using the interatomic potential from [178]. The values thereby obtained were found to be nearly identical to the interaction distance obtained by applying eq. (30) to loops of 61 to 331 SIA, augmented by the value of the capture radius for the single interstitial (again with $R_{FP} = 3.3a_0$). This suggests that, at least along the radial direction, the approach leading to eq. (30) is reasonable, while pointing to the fact that the choice $R_{FP} = 3.3a_0$ is more appropriate than $2.26a_0$, despite the fact that the latter was obtained from atomistic calculations [175] and also agrees with one [171] of the two [171,172] experimental assessments that we have knowledge of. The use of eq. (30) for the description of ⟨100⟩ loops is questionable. However, as briefly discussed in Appendix A.3, since the concept of capture radius is itself an approximation, eq. (30) can be considered fairly acceptable in that case, too. In this context, the Supplementary Material includes a brief discussion of the numerical differences between capture radii for vacancy clusters and self-interstitial loops and proposes an approach that may be tested.

Fig. 15 (right side) shows pictorially that, above a certain loop size, the inner region will remain unaffected by the presence of the loop and

Fig. 15. Pictorial illustration of the strain fields associated with a dislocation loop, depending on size and description. On the left side, we illustrate the description that is implicitly assumed when using eq. (30) for the capture radius : the loop is represented by the blue area; the strain field associated with the loop is described by a sphere, the radius of which is somewhat smaller than the actual extension of the loop strain field in the radial direction, if associated with the radial distance where the pressure goes to zero. The sphere also underestimates the extension of the strain field in the direction normal to the habit plane, which is illustrated pictorially in the central figure. On the right side, when the loop is large enough, the central part is not deformed
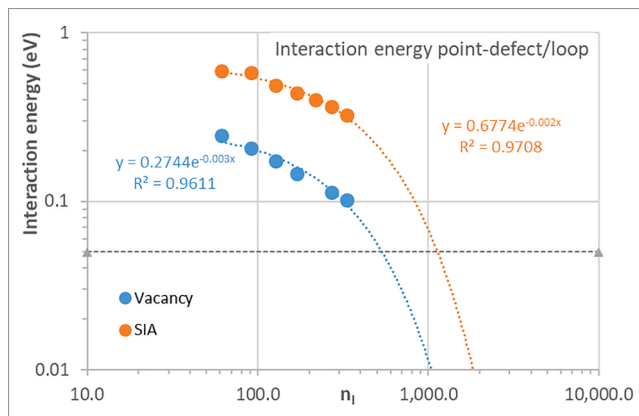
and corresponds to a perfect lattice. When this limit is reached, the shape to be associated with the strain field is better described by a torus. (For interpretation of the references to colour in this figure legend, the reader is referred to the web version of this article.)

Fig. 16. Extrapolation to approach zero of data points obtained as in [179] for the attractive and repulsive interaction energy between, respectively, a vacancy or a self-interstitial and a loop, when the former are located on the habit plane of the loop at the geometrical centre of it. The horizontal dashed line indicates the limit used to consider that the interaction energy becomes negligible.

its strain field will thus become better described by a torus. It is however not obvious how to assign a threshold size above which the switch from a spherical to a toroidal shape should occur. This is because, in reality, with increasing size the strain field changes gradually from being elongated in the direction normal to the loop habit plane, to taking a progressively flatter shape. The latter becomes increasingly thinned at the centre for sufficiently large size, but without any clearcut threshold. The difficulty of defining a threshold is exacerbated by the variability of the results of strain field characteristic distance calculations depending on the atomistic details and on the criteria used, as emerges from Table 4. In [10,11] the threshold was arbitrarily set to 150 self-interstitials. Here we try an estimate by using calculations of the interaction energy between a single vacancy and a single self-interstitial and the loop, when the point defect is located along the normal to the loop habit plane that passes through the loop centre, as a function of the loop size. The details of how the calculations have been performed can be found in [179]. It should be noted that the interaction is attractive in the case of the single vacancy, because the region is compressed and compression is eased by this defect, while in the case of the single self-interstitial repulsion occurs, because this defect compresses the lattice like the loop does, at least in certain directions. However, for the present purpose this is irrelevant, as what we want to know is for which loop size either the attraction or the repulsion vanish, because at that point the centre of the loop can be considered as coincident with the perfect lattice, i.e. the point defect could migrate through the loop without noticing its presence (and vice versa). Fig. 16 shows the moduli of the interaction energy data points as functions of loop size, extrapolated with a rapidly decaying exponential function. This figure suggests that, depending on which elastic interaction energy value is considered to be negligibly small (between 0.05 and 0.01), a vacancy would cease to feel the strain field at the centre of the loop only for radii that exceed 3–6 nm, i.e. containing well in excess of 500–2000 SIA. In the case of the interaction with a single SIA, the threshold size is even bigger. Thus, based on this argument, the toroidal shape would only be justified for significantly large dislocation loops.

To conclude, we show examples from the literature of Scheme B. For instance in [8] the capture radius between two defects i and j, r_{ij}, is defined as:

$$r_{ij}(n_i, n_j) = Z_{ij}[r_i(n_i) + r_j(n_j) + d_{ij}] \qquad (34)$$

where r_i and r_j are the geometrical radii of each defect, calculated assuming a spherical volume, as follows:

$$r_i(n) = a_0 \left(\frac{3n_i}{8\pi}\right)^{\frac{1}{3}} \qquad (35)$$

Z_{ij} is the bias that effectively takes into account the elastic interaction between defects: the capture radius between self-interstitials will be larger, through a bias factor, than between vacancies, and intermediate in case of recombination, due to their more extended elastic field. The distance d_{ij} is fitted to R_{FP}. While the concept behind eqs. (34) and (35) is very similar to the above example of scheme A from [6] (eq. (28)), here both involved defects enter the definition of capture radius, so this is an example of Scheme B.

In [13] the capture radius was defined taking inspiration from eq. (27), thus a point-defect and a cluster will interact when their mutual distance is equal to, or less than:

$$r_{ij}(n) = r_i(n) + \delta_{ij} \qquad (36)$$

where $r_i(n)$ is given by eq. (35), as well, and δ_{ij} accounts for the bias, i.e. it can be chosen to equal the second nearest neighbour (2nn) distance in the case of interaction between a void and a vacancy, but the 3nn in the interaction between a loop and a self-interstitial. It is emphasised that any Scheme A can be easily translated into a Scheme B, by using the corresponding equations for $r_k(n)$ and tuning the d_{ij} or δ_{ij} term; *a priori* the other way round is not guaranteed. No systematic sensitivity study has been performed so far to evaluate which scheme or choice work better when applied to specific cases, especially comparing with experiments.

Concluding remarks

In this paper we have explored the most important parameters that define the mobility and stability of radiation defects in α-Fe (vacancies and self-interstitials and especially their clusters), as well as their mutual interaction, as currently used in object kinetic Monte Carlo simulations of microstructure evolution under irradiation, based on the available literature and a few data and considerations of our own. We also spent a few words on how the main sinks and traps can be included in the model. In some cases the important mechanisms and parameters can be said to be fairly established. For example concerning the mobility and also the stability of vacancy clusters, the convergence of several different approaches gives a certain confidence that the parameters that we currently use are at least reasonable and fairly complete. However, especially for what concerns self-interstitials, but also extended sinks, many open questions remain; for instance:

1. The fraction, unfaulting energy and effective mobility (if any) of small self-interstitial clusters in non-parallel configurations (C15) remain largely unknown. This lack of knowledge prevents models from including explicitly these defects and treating them as a separate class of objects that may transform into other ones, as should be done in principle, thereby casting large and currently unquantifiable uncertainties on the description of the effective mobility of self-interstitial clusters that is adopted in existing models. Clearly the problem here comes from the fact that interatomic potentials do not manage to reproduce correctly the relative stability of the different possible configurations of small clusters (parallel and non-parallel). Hopefully, the increasingly widespread use of DFT-based molecular dynamics and in any case the augmentation of the number of atoms that can be affordably simulated will fill this gap in the near future.

2. The mobility and mechanisms of formation of ⟨100⟩ loops remain only tentatively parameterised. In most models ⟨100⟩ loops are considered to be immobile, since they can be observed under TEM and are thus assumed not to migrate away. However, some experimental observations seem to point to the possible migration of these defects at either high temperatures and/or high doses, at least for thin films. Therefore, more precise migration energy values for these

defects are needed. Concerning the formation of ⟨100⟩ loops, it is established that there are at least two non-mutually excluding mechanisms, namely reactions between ½⟨111⟩ loops and transformation of C_{15} clusters, but the introduction of these mechanisms involves many arbitrary decisions, such as the size range of reactions between ½⟨111⟩ loops leading to ⟨100⟩ formation or the fraction of C_{15} clusters that are created in cascades and the fraction of these that grows into ⟨100⟩ loops. In addition, other mechanisms are possible, such as direct transformation of a ½⟨111⟩ loop into a ⟨100⟩ loop [104], or even the unlikely, but not impossible, concomitant reaction of three loops [180], for which it is hard to imagine how to define the conditions of occurrence. The relative mobility of ⟨100⟩ versus ½⟨111⟩ loops, together with the outcome of interactions between loops of similar and different type and the role of non-parallel configurations, are all expected to be key to determine the experimentally observed ratio between ⟨100⟩ and ½⟨111⟩ loop populations. On the other hand, one question that should be asked is how important it is to reproduce this ratio correctly, in connection with the assessment of the effect of the microstructure on macroscopic property changes such as hardening, embrittlement or swelling: at the current level of knowledge the opinions on this point can be very different.

3. Which mobile defects are absorbed or trapped at dislocations in the absence of applied strain is also an important question that did not receive a lot of attention, except e.g. in [116]. (As a matter of fact, except for ref. [116], all studies of defect absorption by dislocations consider the case of a moving dislocation under applied strain). Allowing explicitly for elastic interactions can help several problems to be solved in terms of range of interaction and possibly also configuration taken by the defect [112–118], in a cost and benefit trade-off, but whether or not and in which size and temperature range absorption or trapping occur is likely to require dynamic atomistic studies. The problem here, like in the case of dislocation/ defect interaction when strain is applied, is the vast number of cases that should be hypothetically studied. Thus approximate solutions will be unavoidable still for some time. The spherical absorber solution proposed here is of easy implementation, but severely limits the predictive capability of models, totally impeding the prediction of heterogeneous distributions of defects, which may have important consequences on the macroscopic properties of the material (e.g. source hardening [138])

These are not the only open questions, though. Grain boundaries and in general interfaces between crystals of several types, from twins to interlayers, are obviously not just insaturable sinks, as they are assumed to be in the vast majority of cases, but rather structures that may interact in a wide variety of ways with radiation defects [181]. These details are currently far from being introduced in any reasonable way in microstructure evolution models, at least not in models that cover a time and space range that allows direct comparison with experiments, such as is the case of OKMC or cluster dynamics models.

Finally, it is quite clear that a possibly even larger complexity is introduced by the presence of (unwanted or unavoidable) impurities and/or (purposefully added) solutes:

4. Formation, mobility and stability of carbon/point-defect complexes. These complexes are known to be formed, to be stable and to interact with each other and with point-defect clusters [152–161]. (The same is also true in fact for other interstitial impurities, such as N and O [158,159]). This interaction has a very significant effect on the microstructure evolution: experiments and simulations alike suggest that, without these impurities, the accumulation of radiation damage would be very limited. Although there is a large list of values for different carbon-vacancy or carbon-self-interstitial complexes, a vast number of gaps remain in our knowledge. In addition, interstitial impurities such as C migrate on their own and thus redistribute themselves in a different way depending on both the pre-existing microstructure (ferritic, martensitic, …), characterized by different dislocation and grain boundary densities, and the possibility or not of forming carbides: these effects should be somehow accounted for in the model.

5. Decoration of radiation defects with solutes in Fe alloys. It is by now established that several substitutional solute atoms are dragged to point-defect clusters by single point-defects [148,182–169] and accumulate there [23,109]. This mechanism not only leads to heterogeneous nucleation of solute clusters, that may evolve to precipitates, and to segregation at extended defects, but also influences enormously the microstructure evolution in terms of type of defects that should be observed under the microscope or with other experimental techniques [23,182–169]. Number density and size distribution of loops and voids change because of the presence of solutes and the properties of solute decorated loops and solute–vacancy clusters become crucial to understand several macroscopic effects. Paradoxically, it is possible that the formation of solute/point-defect complexes will reduce the need for a detailed knowledge of the properties of, for example, self-interstitial clusters and loops in pure Fe, because eventually the effect of the solute decoration will be dominant, thereby blurring other effects [23].

The current knowledge on these last two aspects will be the focus of the follow up papers to this work.

Declaration of Competing Interest

The authors declare that they have no known competing financial interests or personal relationships that could have appeared to influence the work reported in this paper.

Appendices.

A1. Heuristic demonstration of the scaling of the attempt frequency for vacancy cluster migration with cluster size (eq. (20))

For a void, the jump frequency (eq. (4)) can be written as

$$\Gamma^{void} = \nu_m^{void} exp\left(\frac{-E_m^{void}}{kT}\right) \tag{A.1}$$

where ν_m^{void} is the attempt frequency for the void to jump and E_m^{void} is the migration energy of the void. Also, from eq. (5):

$$\Gamma^{void} = \frac{6D^{void}}{d_j^2} \tag{A.2}$$

where D^{void} is the diffusion coefficient for a void. Following Golubov *et al.* [168], the diffusion coefficient of a void can by written as

$$D^{void} = \frac{3}{2\pi} D_s \left(\frac{\Omega^{1/3}}{r}\right)^4 \tag{A.3}$$

where $D_s = D_s^0 \exp\left(\frac{-E_s}{kT}\right)$ is the surface diffusion coefficient, $\Omega = \frac{a_0^3}{2}$ is the atomic volume and

$$r = \left(\frac{3N_v\Omega}{4\pi}\right)^{1/3} = \left(\frac{3N_v}{8\pi}\right)^{1/3} a_0 \tag{A.4}$$

the mean radius of a vacancy cluster (void) with N_v vacancies. This comes from assuming that the volume of the vacancy cluster equals the volume of a sphere with radius r. The diffusion coefficient may now be rewritten as

$$D^{void} = \frac{3}{2\pi} \left(\frac{4\pi}{3N_v}\right)^{4/3} D_s^0 exp\left(\frac{-E_s}{kT}\right) \tag{A.5}$$

and the jump frequency as

$$\Gamma^{void} = \frac{9}{\pi d_j^2} \left(\frac{4\pi}{3N_v}\right)^{4/3} D_s^0 exp\left(\frac{-E_s}{kT}\right) \tag{A.6}$$

Assuming, now, that the migration energy of the void, E_m^{void}, is in fact given by the migration energy of the surface of the vacancy cluster, E_s, by identifying eqs. (A.2) and (A.6) one gets that

$$\nu_m^{void} = \frac{9}{\pi d_j^2} \left(\frac{4\pi}{3N_v}\right)^{4/3} D_s^0 = \frac{9}{\pi d_j^2} \left(\frac{4\pi}{3}\right)^{4/3} D_s^0 \left(\frac{1}{N_v}\right)^{4/3} \tag{A.7}$$

Here, neglecting constants on the order of unities, the quantity $= \frac{9}{\pi d_j^2}\left(\frac{4\pi}{3}\right)^{4/3}D_s^0$ is an attempt frequency that, lacking better estimates, can be expressed in units of ν_{m1}, so it make sense to write that

$$\nu_m \sim \frac{\nu_{m1}}{N_v^{4/3}} \tag{A.8}$$

A2. Heuristic demonstration of the scaling of the attempt frequency for vacancy emission from a cluster with cluster size (eq. (25))

For any given first order reaction $A + B \Leftrightarrow C$, with k^+ and k^- the forward and backward reaction constants, the following relationship holds [183]:

$$k^- = k^+ N_s exp\left(\frac{-E_b}{kT}\right) \tag{A.9}$$

where N_s is the density of the material ($8.46\cdot10^{22}cm^{-3}$ in Fe), E_b is the binding energy of the reaction, and:

$$k^+ = 4\pi r D_V \tag{A.10}$$

(absorption rate, related to the sink strength for absorption of a 3D migrating defect; here a vacancy, thus the subscript $_V$). This gives:

$$k^- = 4\pi r D_V N_s exp\left(\frac{-E_b}{kT}\right) \tag{A.11}$$

And, using eqs. (2)-(5)

$$D_V = D_0^V \exp\left(\frac{-E_m}{kT}\right) \tag{A.12}$$

Which, once replaced in eq. (A.11), gives

$$k^- = 4\pi r D_0^V N_s exp\left(\frac{-E_b - E_m}{kT}\right) = 4\pi r D_0^V N_s exp\left(\frac{-E_d}{kT}\right) \tag{A.13}$$

The atomic density is $\Omega = \frac{a_0^3}{2}$, thus:

$$\frac{4}{3}\pi r^3 = n\Omega = \frac{na_0^3}{2} \Rightarrow r = \left(\frac{3n}{8\pi}\right)^{1/3} a_0 \tag{A.14}$$

The diffusion prefactor, eq. (3), is defined as

$$D_0^V = \frac{f_c d_j^2 \nu_m(1)}{6}$$
(A.15)

where $f_c \approx 1$ is the correlation factor, $d_j = \frac{\sqrt{3}}{2} a_0$ is the single jump distance and $\nu_m(1)$ is known. Thus:

$$k^- = \pi \left(\frac{3n}{8\pi}\right)^{1/3} f_c \nu_m(1) exp\left(\frac{-E_d}{kT}\right)$$
(A.16)

which equals

$$k^- = \Gamma(T) = \nu_e exp\left(\frac{-E_d}{kT}\right)$$
(A.17)

from which:

$$\nu_e(n) = \pi \left(\frac{3}{8\pi}\right)^{\frac{1}{3}} f \nu_m(1) n^{1/3} \Rightarrow \nu_e \approx 1.5 \nu_m(1) n^{1/3}$$
(A.18)

A3. Different ways to estimate the radius of an hexagonal ½⟨111⟩ dislocation loop in the bcc lattice

The radius of a loop can be calculated in two different ways. One can be understood with the help of Fig. A.1, which represents on a {111} plane the smallest perfect ½⟨111⟩ loop, composed by 7 SIAs located on three different atomic planes, each identified by different geometrical shapes.

It consists in taking as radius r_l of the loop the distance AC between the centre and the vertex of the regular hexagon identified by the atomic positions on the crystallographic {111} plane in Fig. A.1. This procedure is unambiguous only in the case of the perfect loops (7, 19, 37, 61, 91. 127, … SIA), i.e. loops that really complete the external layer of the hexagon. If L is the number of complete hexagonal layers, the number of SIA in the corresponding perfect loop, n_{pl}, is
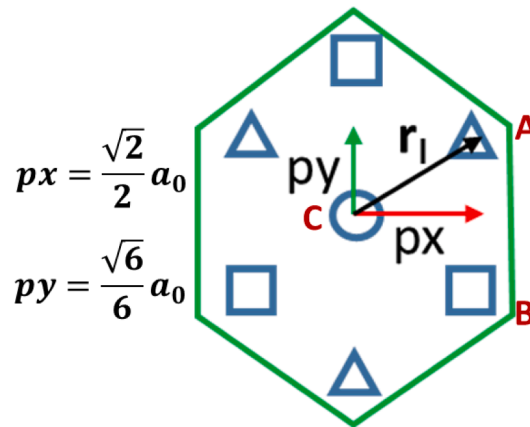

Fig. A1. The smallest perfect ½⟨111⟩ loop (7 SIA) represented on the {111} crystallographic plane, formed by SIA located on three atomic planes, indicated by different geometrical figures. The distances indicated on the figure are used in the text to calculate the radius of the loop.

$$n_{pl}(L) = 1 + 6 \sum_1^L k$$
(A.19)

which gives the above series of values. The corresponding radii, calculated as in Fig. A.1, as functions of the number of complete hexagonal layers L, are:

$$r_{pl}(L) = a_0 L \sqrt{px^2 + py^2} = \sqrt{\frac{2}{3}} a_0 L$$
(A.20)

By interpolating the curve $r_{pl}(n_{pl})$ with a power function one gets, for any n (number of defects in the loop):

$$r_l(n) \cong 0.299 a_0 n^{0.57}$$
(A.21)

Which concides with eq. (32).

Alternatively, a specific surface S_I is associated with each SIA in the loop. With reference to Fig. A.1, this surface equals the triangle ABC, the area of which is $a_0^2/\sqrt{3}$. The radius of a loop of n SIA can then be obtained by identifying its overall surface to a circle (similarly to the identification between the sum of the volumes of vacancies in a cluster with a sphere):
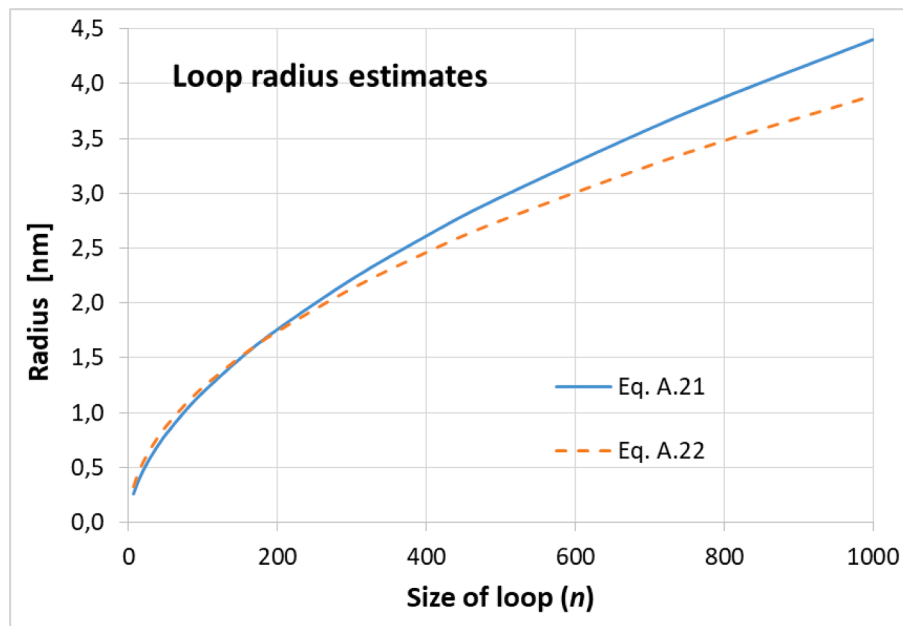
Fig. A2. Estimates of the radius of a ½⟨1 1 1⟩ loop according to the two approximations discussed in the text.

$$\pi r_I^2 = n \frac{a_0^2}{\sqrt{3}} \rightarrow r_I(n) = a_0 \sqrt{\frac{n}{\pi\sqrt{3}}} \cong 0.429 a_0 n^{0.5} \tag{A.22}$$

The latter expression has been used to obtain eqs. (30) and (33). Eqs. (A.21) and (A.22) give obviously different numerical values, but are overall very similar: the former yields slightly smaller values for small loops, but somewhat larger values for larger ones, because of the slightly larger exponent in the power law, as can be appreciated in Fig. A.2.

The use of eq. (30) for the description of ⟨1 0 0⟩ loops is clearly questionable. In practice, however, since the concept of capture radius is in itself an approximation, eq. (30) can be considered fairly acceptable in that case, too. Following the same idea as in eq. (A.22), but with the area per SIA associated with a ⟨1 0 0⟩ loop, it turns out that the denominator $\sqrt{\pi\sqrt{3}}$ is replaced by $\sqrt{2\pi}$, which numerically has very similar value, thus the main approximation consists in assigning a circular geometry to loop that are in fact rectangular. It is possible to take into account explicitly the rectangular geometry of ⟨1 0 0⟩ loops and to estimate their size in terms of its half-diagonal, and derive from there an equation equivalent to eq. (A.21). To our knowledge, however, the latter level of refinement has never been applied in any OKMC model that makes use of a capture radius approach.

Appendix B. Supplementary data

Supplementary data to this article can be found online at https://doi.org/10.1016/j.nme.2021.101069.

References

[1] F. Gao, D.J. Bacon, A.V. Barashev, H.L. Heinisch. Kinetic Monte Carlo Annealing Simulation of Damage Produced by Cascades in Alpha-Iron. MRS Online Proceedings Library Archive, Vol. 540: Symposium N / Microstructural Processes in Irradiated Materials, 1998, 703-708. DOI: 10.1557/PROC-540-703.

[2] N. Soneda, T.D. de la Rubia, Defect production, annealing kinetics and damage evolution in α-Fe: an atomic-scale computer simulation, Philos. Mag. A 78 (5) (1998) 995–1019, https://doi.org/10.1080/01418619808239970.

[3] N. Soneda, T. Diaz de La Rubia, Migration kinetics of the self-interstitial atom and its clusters in bcc Fe, Philos. Mag. A 81 (2) (2001) 331–343, https://doi.org/10.1080/01418610108214307.

[4] M.J. Caturla, N. Soneda, E. Alonso, B.D. Wirth, T. Díaz de la Rubia, J.M. Perlado, Comparative study of radiation damage accumulation in Cu and Fe, J. Nucl. Mater. 276 (1-3) (2000) 13–21.

[5] N. Soneda, S. Ishino, A. Takahashi, K. Dohi, Modeling the microstructural evolution in bcc-Fe during irradiation using kinetic Monte Carlo computer simulation, J. Nucl. Mater. 323 (2-3) (2003) 169–180.

[6] C. Domain, C.S. Becquart, L. Malerba, Simulation of radiation damage in Fe alloys: an object kinetic Monte Carlo approach, J. Nucl. Mater. 335 (1) (2004) 121–145, https://doi.org/10.1016/j.jnucmat.2004.07.037.

[7] H. Xu, Y.N. Osetsky, R.E. Stoller, Cascade annealing simulations of bcc iron using object kinetic Monte Carlo, J. Nucl. Mater. 423 (1-3) (2012) 102–109, https://doi.org/10.1016/j.jnucmat.2012.01.020.

[8] C. Björkas, K. Nordlund, M.J. Caturla, Influence of the picosecond defect distribution on damage accumulation in irradiated α-Fe, Phys. Rev. B 85 (2012), 024105, https://doi.org/10.1103/PhysRevB.85.024105.

[9] I. Martin-Bragado, A. Rivera, G. Valles, J.L. Gomez-Selles, M.J. Caturla, MMonCa: An Object Kinetic Monte Carlo simulator for damage irradiation evolution and defect diffusion, Comput. Phys. Commun. 184 (12) (2013) 2703–2710, https://doi.org/10.1016/j.cpc.2013.07.011.

[10] V. Jansson, M. Chiapetto, L. Malerba, The nanostructure evolution in Fe–C systems under irradiation at 560 K, J. Nucl. Mater. 442 (1-3) (2013) 341–349, https://doi.org/10.1016/j.jnucmat.2013.09.017.

[11] V. Jansson, L. Malerba, Simulation of the nanostructure evolution under irradiation in Fe–C alloys, J. Nucl. Mater. 443 (1-3) (2013) 274–285, https://doi.org/10.1016/j.jnucmat.2013.07.046.

[12] D. Terentyev, I. Martin-Bragado, Evolution of dislocation loops in iron under irradiation: The impact of carbon, Scr. Mater. 97 (2015) 5–8, https://doi.org/10.1016/j.scriptamat.2014.10.021.

[13] F. Jiménez, C.J. Ortiz, A GPU-based parallel Object kinetic Monte Carlo algorithm for the evolution of defects in irradiated materials, Comput. Mater. Sci. 113 (2016) 178–186, https://doi.org/10.1016/j.commatsci.2015.11.011.

[14] J.P. Balbuena, M.J. Aliaga, I. Dopico, M. Hernández-Mayoral, L. Malerba, I. Martin-Bragado, M.J. Caturla, Insights from atomistic models on loop nucleation and growth in α -Fe thin films under Fe⁺ 100 keV irradiation, J. Nucl. Mater. 521 (2019) 71–80, https://doi.org/10.1016/j.jnucmat.2019.04.030.

[15] M. Chiapetto, L. Malerba, C.S. Becquart, Nanostructure evolution under irradiation in FeMnNi alloys: A "grey alloy'' object kinetic Monte Carlo model, J. Nucl. Mater. 462 (2015) 91–99, https://doi.org/10.1016/j.jnucmat.2015.03.045.

[16] M. Chiapetto, L. Malerba, C.S. Becquart, Effect of Cr content on the nanostructural evolution of irradiated ferritic/martensitic alloys: An object kinetic Monte Carlo model, J. Nucl. Mater. 465 (2015) 326–336, https://doi.org/10.1016/j.jnucmat.2015.06.012.

[17] M. Chiapetto, C.S. Becquart, C. Domain, L. Malerba, Nanostructure evolution under irradiation of Fe(C)MnNi model alloys for reactor pressure vessel steels, Nucl. Instrum. Method. Phys. Res. B 352 (2015) 56–60, https://doi.org/10.1016/j.nimb.2014.11.102.

[18] M. Chiapetto, C.S. Becquart, C. Domain, L. Malerba, Kinetic Monte Carlo simulation of nanostructural evolution under post-irradiation annealing in dilute FeMnNi, Phys. Status Solidi C 12 (1–2) (2015) 20–24, https://doi.org/10.1002/pssc.201400143.

[19] M. Chiapetto, L. Malerba, C.S. Becquart, Simulation of nanostructural evolution under irradiation in Fe-9%Cr –C alloys: An object kinetic Monte Carlo study of the effect of temperature and dose-rate, Nucl. Mater. Energy 9 (2016) 565–570, https://doi.org/10.1016/j.nme.2016.04.009.

[20] M. Chiapetto, L. Malerba, A. Puype, C.S. Becquart, Object kinetic Monte Carlo study of the effect of grain boundaries in martensitic Fe–Cr–C alloys, Phys. Status Solidi A 213 (11) (2016) 2981–2987, https://doi.org/10.1002/pssa.201600294.

[21] M. Chiapetto, L. Messina, C.S. Becquart, P. Olsson, L. Malerba, Nanostructure evolution of neutron-irradiated reactor pressure vessel steels: Revised Object kinetic Monte Carlo model, Nucl. Instrum. Method. Phys. Res. B 393 (2017) 105–109, https://doi.org/10.1016/j.nimb.2016.09.025.

[22] M. Chiapetto, Computer simulation of the nanostructural evolution under irradiation in ferritic alloys, PhD. Thesis (defended in 2017), University of Lille, France, 2018.

[23] N. Castin, G. Bonny, A. Bakaev, F. Bergner, C. Domain, J.M. Hyde, L. Messina, B. Radiguet, L. Malerba, The dominant mechanisms for the formation of solute-rich clusters in low-Cu steels under irradiation, Mater. Today Energy 17 (2020) 100472, https://doi.org/10.1016/j.mtener.2020.100472.

[24] H. Xu, Y.N. Osetsky, R.E. Stoller, Simulating complex atomistic processes: On-the-fly kinetic Monte Carlo scheme with selective active volumes, Phys. Rev. B 84 (2011), 132103, https://doi.org/10.1103/PhysRevB.84.132103.

[25] H. Xu, R.E. Stoller, Y.N. Osetsky, Cascade defect evolution processes: Comparison of atomistic methods, J. Nucl. Mater. 443 (1-3) (2013) 66–70, https://doi.org/10.1016/j.jnucmat.2013.07.001.

[26] H. Xu, R.E. Stoller, Y.N. Osetsky, D. Terentyev, Solving the Puzzle of <100> Interstitial Loop Formation in bcc Iron, Phys. Rev. Lett. 110 (2013), 265503, https://doi.org/10.1103/PhysRevLett.110.265503.

[27] L.K. Béland, P. Brommer, F. El-Mellouhi, J.-F. Joly, N. Mousseau, Kinetic activation-relaxation technique, Phys. Rev. E 84 (4) (2011), https://doi.org/10.1103/PhysRevE.84.046704.

[28] E. Machado-Charry, L.K. Béland, D. Caliste, L. Genovese, T. Deutsch, N. Mousseau, P. Pochet, Optimized energy landscape exploration using the ab initio based activation-relaxation technique, J. Chem. Phys. 135 (3) (2011) 034102, https://doi.org/10.1063/1.3609924.

[29] Y.N. Osetsky, L.K. Béland, A.V. Barashev, Y. Zhang, On the existence and origin of sluggish diffusion in chemically disordered concentrated alloys, Curr. Opin. Solid State Mater. Sci. 22 (3) (2018) 65–74, https://doi.org/10.1016/j.cossms.2018.05.003.

[30] R.E. Stoller, S.I. Golubov, C. Domain, C.S. Becquart, Mean field rate theory and object kinetic Monte Carlo: A comparison of kinetic models, J. Nucl. Mater. 382 (2-3) (2008) 77–90, https://doi.org/10.1016/j.jnucmat.2008.08.047.

[31] C.S. Becquart, A. Barbu, J.L. Bocquet, M.J. Caturla, C. Domain, C.-C. Fu, S. I. Golubov, M. Hou, L. Malerba, C.J. Ortiz, A. Souidi, R.E. Stoller, Modeling the long-term evolution of the primary damage in ferritic alloys using coarse-grained methods, J. Nucl. Mater. 406 (1) (2010) 39–54, https://doi.org/10.1016/j.jnucmat.2010.05.019.

[32] L. Malerba, Molecular dynamics simulation of displacement cascades in α-Fe: A critical review, J. Nucl. Mater. 351 (1-3) (2006) 28–38, https://doi.org/10.1016/j.jnucmat.2006.02.023.

[33] R.E. Stoller, "Primary Radiation Damage Formation," in Comprehensive Nuclear Materials, ed. R.J.M. Konings, Chapter 1.11 (Elsevier Ltd.), 2012, 293-332.

[34] K. Nordlund, S.J. Zinkle, A.E. Sand, F. Granberg, R.S. Averback, R.E. Stoller, T. Suzudo, L. Malerba, F. Banhart, W.J. Weber, F. Willaime, S.L. Dudarev, D. Simeone, Primary radiation damage: A review of current understanding and models, J. Nucl. Mater. 512 (2018) 450–479, https://doi.org/10.1016/j.jnucmat.2018.10.027.

[35] M.R. Gilbert, J.-C. Sublet, Differential dpa calculations with SPECTRA-PKA, J. Nucl. Mater. 504 (2018) 101–108, https://doi.org/10.1016/j.jnucmat.2018.03.032.

[36] R.E. Stoller, M.B. Toloczko, G.S. Was, A.G. Certain, S. Dwaraknath, F.A. Garner, On the use of SRIM for computing radiation damage exposure, Nucl. Instrum. Method. Phys. Res. B 310 (2013) 75–80, https://doi.org/10.1016/j.nimb.2013.05.008.

[37] C.J. Ortiz, A. Souidi, C.S. Becquart, C. Domain, M. Hou, Recent radiation damage studies and developments of the Marlowe code, Radiat Eff. Defects Solids 169 (7) (2014) 592–602, https://doi.org/10.1080/10420150.2014.920018.

[38] R.E. Stoller, L.R. Greenwood, Subcascade formation in displacement cascade simulations: Implications for fusion reactor materials, J. Nucl. Mater. 271&272 (1999) 57–62, https://doi.org/10.1016/S0022-3115(98)00730-2.

[39] M.J. Norgett, M.T. Robinson, I.M. Torrens, A proposed method of calculating displacement dose rates, Nucl. Eng. Des. 33 (1) (1975) 50–54, https://doi.org/10.1016/0029-5493(75)90035-7.

[40] K. Nordlund, S.J. Zinkle, A.E. Sand, F. Granberg, R.S. Averback, R. Stoller, T. Suzudo, L. Malerba, F. Banhart, W.J. Weber, F. Willaime, S.L. Dudarev, D. Simeone, Improving atomic displacement and replacement calculations with physically realistic damage models, Nat. Commun. 9 (1) (2018), https://doi.org/10.1038/s41467-018-03415-5.

[41] P. Olsson, C.S. Becquart, C. Domain, Ab initio threshold displacement energies in iron, Mater. Res. Lett. 4 (4) (2016) 219–225, https://doi.org/10.1080/21663831.2016.1181680.

[42] A. Souidi, C.S. Becquart, C. Domain, D. Terentyev, L. Malerba, A.F. Calder, D. J. Bacon, R.E. Stoller, Y.N. Osetsky, M. Hou, Dependence of radiation damage accumulation in iron on underlying models of displacement cascades and subsequent defect migration, J. Nucl. Mater. 355 (1-3) (2006) 89–103, https://doi.org/10.1016/j.jnucmat.2006.04.009.

[43] A. Souidi, M. Hou, C.S. Becquart, L. Malerba, C. Domain, R.E. Stoller, On the correlation between primary damage and long-term nanostructural evolution in iron under irradiation, J. Nucl. Mater. 419 (1-3) (2011) 122–133, https://doi.org/10.1016/j.jnucmat.2011.08.049.

[44] Singh B.N. Impacts of damage production and accumulation on materials performance in irradiation environment. J. Nucl. Mater. 258-263 (part I), 18–29. 1998, DOI: 10.1016/S0022-3115(98)00264-5.

[45] L. Huang, T. Schuler, M. Nastar, Atomic-scale modeling of the thermodynamic and kinetic properties of dilute alloys driven by forced atomic relocations, Phys. Rev. B 100 (2019), 224103, https://doi.org/10.1103/PhysRevB.100.224103.

[46] K. Vörtler, N. Juslin, G. Bonny, L. Malerba, K. Nordlund, J. Phys.: Condens. Matter 23 (2011), 355007, https://doi.org/10.1088/0953-8984/23/35/355007].

[47] M.R. Gilbert, S.L. Dudarev, P.M. Derlet, D.G. Pettifor, Structure and metastability of mesoscopic vacancy and interstitial loop defects in iron and tungsten, J. Phys.: Condens. Matter 20 (34) (2008) 345214, https://doi.org/10.1088/0953-8984/20/34/345214.

[48] M.R. Gilbert, Z. Yao, M.A. Kirk, M.L. Jenkins, S.L. Dudarev, Vacancy defects in Fe: Comparison between simulation and experiment, J. Nucl. Mater. 386–388 (2009) 36–40, https://doi.org/10.1016/j.jnucmat.2008.12.055.

[49] M.J. Aliaga, R. Schäublin, J.F. Löffler, M.J. Caturla, Surface-induced vacancy loops and damage dispersion in irradiated Fe thin films, Acta Mater. 101 (2015) 22–30, https://doi.org/10.1016/j.actamat.2015.08.063.

[50] N. Soneda, S. Ishino, T. Díaz de la Rubia, Vacancy loop formation by 'cascade collapse' in α-Fe: a molecular dynamics study of 50 keV cascades, Philos. Mag. Lett. 81 (9) (2001) 649–659, https://doi.org/10.1080/09500830110062799.

[51] A.E. Sand, J. Byggmästar, A. Zitting, K. Nordlund, Defect structures and statistics in overlapping cascade damage in fusion-relevant bcc metals, J. Nucl. Mater. 511 (2018) 64–74, https://doi.org/10.1016/j.jnucmat.2018.08.049.

[52] M.L. Jenkins, C.A. English, B.L. Eyre, Heavy-ion irradiation of α -iron, Philos. Mag. A 38 (1) (1978) 97–114, https://doi.org/10.1080/01418617808239220.

[53] YU.N. Osetsky, D.J. Bacon, A. Serra, Thermally activated glide of small dislocation loops in metals, Philos. Mag. Lett. 79 (5) (1999) 273–282, https://doi.org/10.1080/095008399177345.

[54] D. Kulikov, L. Malerba, M. Hou, On the binding energies and configurations of vacancy and copper–vacancy clusters in bcc Fe–Cu:a computational study, Phil. Mag. 86 (2) (2006) 141–172, https://doi.org/10.1080/14786430500156930.

[55] D. Kandaskalov, C. Mijoule, D. Connétable, Study of multivacancies in alpha Fe, J. Nucl. Mater. 441 (1-3) (2013) 168–177, https://doi.org/10.1016/j.jnucmat.2013.05.030.

[56] C.S. Becquart, C. Domain, Ab initio contribution to the study of complexes formed during dilute FeCu alloys radiation, Nucl. Instrum. Method. Phys. Res. B 202 (2003) 44–50, https://doi.org/10.1016/S0168-583X(02)01828-1.

[57] C.-C. Fu, J. Dalla Torre, F. Willaime, J.-L. Bouquet, A. Barbu, Multiscale modelling of defect kinetics in irradiated iron, Nat. Mater. 4 (2005) 68–74, https://doi.org/10.1038/nmat1286.

[58] L. Malerba, M.C. Marinica, N. Anento, C. Björkas, H. Nguyen, C. Domain, F. Djurabekova, P. Olsson, K. Nordlund, A. Serra, D. Terentyev, F. Willaime, C. S. Becquart, Comparison of empirical interatomic potentials for iron applied to radiation damage studies, J. Nucl. Mater. 406 (1) (2010) 19–38, https://doi.org/10.1016/j.jnucmat.2010.05.017.

[59] N. Castin, M.I. Pascuet, L. Malerba, Mobility and stability of large vacancy and vacancy–copper clusters in iron: An atomistic kinetic Monte Carlo study, J. Nucl. Mater. 429 (1-3) (2012) 315–324, https://doi.org/10.1016/j.jnucmat.2012.06.020.

[60] B. Pannier, Towards the prediction of microstructure evolution under irradiation of model ferritic alloys with a hybrid AKMC-OKMC approach, PhD dissertation, University of Lille, France, 2017.

[61] B.N. Singh, S.I. Golubov, H. Trinkaus, A. Serra, Y.N. Osetsky, A.V. Barashev, Aspects of microstructure evolution under cascade damage conditions, J. Nucl. Mater. 251 (1997) 107–122, https://doi.org/10.1016/S0022-3115(97)00244-4.

[62] S. Takaki, J. Fuss, H. Kuglers, U. Dedek, H. Schultz, The resistivity recovery of high purity and carbon doped iron following low temperature electron irradiation, Radiation Effects 79 (1-4) (1983) 87–122, https://doi.org/10.1080/00337578308207398.

[63] D.A. Terentyev, L. Malerba, M. Hou, Dimensionality of interstitial cluster motion in bcc-iron, Physical Review B 75 (2007), 104108, https://doi.org/10.1103/PhysRevB.75.104108.

[64] N. Anento, A. Serra, Y.N. Osetsky, Atomistic study of multimechanism diffusion by self-interstitial defects in α-Fe. Model. Simulat. Mater. Sci. Eng. 18, 025008. 2010. DOI: 10.1088/0965-0393/18/2/025008.

[65] M.-C. Marinica, F. Willaime, N. Mousseau, Energy landscape of small clusters of self-interstitial dumbbells in iron, Phys. Rev. B 83 (2011), 094119, https://doi.org/10.1103/PhysRevB.83.094119.

[66] D. Terentyev, T.C.P. Klaver, P. Olsson, M.-C. Marinica, F. Willaime, C. Domain, L. Malerba, Self-Trapped Interstitial-Type Defects in Iron, Phys. Rev. Lett. 100 (2008), 145503, https://doi.org/10.1103/PhysRevLett.100.145503.

[67] C.-C. Fu, F. Willaime, P. Ordejón, Stability and Mobility of Mono- and Di-Interstitials in α -Fe, Phys. Rev. Lett. 92 (17) (2004), 175503, https://doi.org/10.1103/PhysRevLett.92.175503.

[68] F. Willaime, C.-C. Fu, M.-C. Marinica, J. Dalla Torre, Stability and mobility of self-interstitials and small interstitial clusters in a-iron: ab initio and empirical potential calculations, Nucl. Instrum. Method. Phys. Res. B 228 (2005) 92–99, https://doi.org/10.1016/j.nimb.2004.10.028.

[69] V. Hivert, R. Pichon, H. Bilger, P. Bichon, J. Verdone, D. Dautreppe, P. Moser, Internal friction in low temperature irradiated bcc metals, J. Phys. Chem. Solids 31 (8) (1970) 1843–1855, https://doi.org/10.1016/0022-3697(70)90176-9.

[70] J. Verdone, W. Chambron, P. Moser, Magnetic anisotropy induced by self-interstitials in low-temperature electron-irradiated iron, Phys. Status Solidi B 61 (1) (1974) K41–K44, https://doi.org/10.1002/(ISSN)1521-395110.1002/pssb:v61:110.1002/pssb:2220610144.

[71] M.-C. Marinica, F. Willaime, J.-P. Crocombette, Irradiation-Induced Formation of Nanocrystallites with C15 Laves Phase Structure in bcc Iron, Phys. Rev. Lett. 108 (2012), 025501, https://doi.org/10.1103/PhysRevLett.108.025501.

[72] L. Dézerald, M.-C. Marinica, L. Ventelon, D. Rodney, F. Willaime, Stability of self-interstitial clusters with C15 Laves phase structure in iron, J. Nucl. Mater. 449 (1-3) (2014) 219–224, https://doi.org/10.1016/j.jnucmat.2014.02.012.

[73] Y. Fan, A. Kushima, B. Yildiz, Unfaulting mechanism of trapped self-interstitial atom clusters in bcc Fe: A kinetic study based on the potential energy landscape, Phys. Rev. B 81 (2010), 104102, https://doi.org/10.1103/PhysRevB.81.104102.

[74] F. Gao, D.J. Bacon, Y.N. Osetsky, P.E.J. Flewitt, T.A. Lewis, Properties and evolution of sessile interstitial clusters produced by displacement cascades in α-iron, J. Nucl. Mater. 276 (1–3) (2000) 213–220, https://doi.org/10.1016/S0022-3115(99)00180-4.

[75] E. Zarkadoula, S.L. Daraszewicz, D.M. Duffy, M.A. Seaton, I.T. Todorov, K. Nordlund, M.T. Dove, K. Trachenko, The nature of high-energy radiation damage in iron, J. Phys.: Condens. Matter 25 (12) (2013) 125402, https://doi.org/10.1088/0953-8984/25/12/125402.

[76] J. Byggmästar, F. Granberg, Dynamical stability of radiation-induced C15 clusters in iron, J. Nucl. Mater. 528 (2020) 151893, https://doi.org/10.1016/j.jnucmat.2019.151893.

[77] J. Byggmästar, F. Granberg, K. Nordlund, Effects of short-range repulsive potential on cascade damage in iron, J. Nucl. Mater. 508 (2018) (2018) 530–539, https://doi.org/10.1016/j.jnucmat.2018.06.005.

[78] B.L. Eyre, R. Bullough, On the formation of interstitial loops in b.c.c. metals, Phil. Mag. 12 (115) (1965) 31–39, https://doi.org/10.1080/14786436508224943.

[79] S.L. Dudarev, R. Bullough, P.M. Derlet, Effect of the α−γ Phase Transition on the Stability of Dislocation Loops in bcc Iron, Phys. Rev. Lett. 100 (2008), 135503, https://doi.org/10.1103/PhysRevLett.100.135503.

[80] R. Alexander, M.-C. Marinica, L. Proville, F. Willaime, K. Arakawa, M.R. Gilbert, S.L. Dudarev, Ab initio scaling laws for the formation energy of nanosized interstitial defect clusters in iron, tungsten, and vanadium, Phys. Rev. B 94 (2016), 024103, https://doi.org/10.1103/PhysRevB.94.024103.

[81] B.D. Wirth, G.R. Odette, D. Maroudas, G.E. Lucas, Dislocation loop structure, energy and mobility of self-interstitial atom clusters in bcc iron, J. Nucl. Mater. 276 (1-3) (2000) 33–40, https://doi.org/10.1016/S0022-3115(99)00166-X.

[82] Y.N. Osetsky, D.J. Bacon, A. Serra, B.N. Singh, S.I. Golubov, Stability and mobility of defect clusters and dislocation loops in metals, J. Nucl. Mater. 276 (1-3) (2000) 65–77, https://doi.org/10.1016/S0022-3115(99)00170-1.

[83] J. Marian, B.D. Wirth, A. Caro, B. Sadigh, G.R. Odette, J.M. Perlado, T. Díaz de la Rubia, Dynamics of self-interstitial cluster migration in pure α -Fe and Fe-Cu alloys, Phys. Rev. B 65 (2002), 144102, https://doi.org/10.1103/PhysRevB.65.144102.

[84] Y.N. Osetsky, D.J. Bacon, A. Serra, B.N. Singh, S.I. Golubov, One-dimensional atomic transport by clusters of self-interstitial atoms in iron and copper, Philos. Mag. A 83 (1) (2003) 61–91, https://doi.org/10.1080/0141861021000016793.

[85] A.V. Barashev, Y.N. Osetsky, D.J. Bacon, Mechanisms of one-dimensional glide of self-interstitial atom clusters in α -iron, Philos. Mag. A 80 (11) (2000) 2709–2720, https://doi.org/10.1080/01418610008216500.

[86] B.L. Eyre, Direct observation of neutron irradiation damage in α-iron, Phil. Mag. 7 (79) (1962) 2107–2113, https://doi.org/10.1080/14786436208214480.

[87] B.L. Eyre, A.F. Bartlett, An electron microscope study of neutron irradiation damage in alpha-iron, Phil. Mag. 12 (116) (1965) 261–272, https://doi.org/10.1080/14786436508218869.

[88] J.S. Bryner, A study of neutron irradiation damage in iron by electron-transmission microscopy, Acta Metall. 14 (3) (1966) 323–336, https://doi.org/10.1016/0001-6160(66)90091-5.

[89] I.M. Robertson, M.L. Jenkins, C.A. English, Low-dose neutron-irradiation damage in α-iron, J. Nucl. Mater. 108–109 (1982) 209–221, https://doi.org/10.1016/0022-3115(82)90489-5.

[90] S.J. Zinkle, B.N. Singh, Microstructure of neutron-irradiated iron before and after tensile deformation, J. Nucl. Mater. 351 (1–3) (2006) 269–284, https://doi.org/10.1016/j.jnucmat.2006.02.031.

[91] A.C. Nicol, M.L. Jenkins, M.A. Kirk, Matrix Damage in Iron, MRS Online Proceedings Library 650 (2000) 13, https://doi.org/10.1557/PROC-650-R1.3.

[92] D.T. Hoelzer, F. Ebrahimi, Effect of Copper and Nickel on the Neutron Irradiation Damage in Iron Alloys. MRS Online Proceedings Library 373: Symposium Y – Microstructure of Irradiated Materials, 1994, 57-62. DOI: 10.1557/PROC-373-57.

[93] I.M. Robertson, M.A. Kirk, W.E. King, Formation of dislocation loops in iron by self-ion irradiations at 40K, Scr. Metall. 18 (4) (1984) 317–320, https://doi.org/10.1016/0036-9748(84)90444-7.

[94] Z. Yao, M. Hernández-Mayoral, M.L. Jenkins, M.A. Kirk, Heavy-ion irradiations of Fe and Fe–Cr model alloys Part 1: Damage evolution in thin-foils at lower doses, Phil. Mag. 88 (21) (2008) 2851–2880, https://doi.org/10.1080/14786430802380469.

[95] M. Hernández-Mayoral, Z. Yao, M.L. Jenkins, M.A. Kirk, Heavy-ion irradiations of Fe and Fe–Cr model alloys Part 2: Damage evolution in thin-foils at higher doses, Phil. Mag. 88 (21) (2008) 2881–2897, https://doi.org/10.1080/14786430802380477.

[96] M.L. Jenkins, Z. Yao, M. Hernández-Mayoral, M.A. Kirk, Dynamic observations of heavy-ion damage in Fe and Fe–Cr alloys, J. Nucl. Mater. 389 (2) (2009) 197–202, https://doi.org/10.1016/j.jnucmat.2009.02.003.

[97] O. El-Atwani, J.E. Nathaniel, A.C. Leff, K. Hattar, M.L. Taheri, Direct Observation of Sink-Dependent Defect Evolution in Nanocrystalline Iron under Irradiation, Scientific Report 7 (2017) 1836, https://doi.org/10.1038/s41598-017-01744-x.

[98] R. Schäublin, B. Décamps, A. Prokhodtseva, J.F. Löffler, On the origin of primary ½a₀<111> and a₀<100> loops in irradiated Fe(Cr) alloys, Acta Mater. 133 (2017) 427–439, https://doi.org/10.1016/j.actamat.2017.02.041.

[99] B.C. Masters, Dislocation loops in irradiated iron, Phil. Mag. 11 (113) (1965) 881–893, https://doi.org/10.1080/14786436508223952.

[100] L.L. Horton, J. Bentley, K. Farrell, A TEM study of neutron-irradiated iron, J. Nucl. Mater. 108–109 (1982) 222–233, https://doi.org/10.1016/0022-3115(82)90490-1.

[101] M. Matijasevic, W. Van Renterghem, A. Almazouzi, Characterization of irradiated single crystals of Fe and Fe-15Cr, Acta Mater. 57 (5) (2009) 1577–1585, https://doi.org/10.1016/j.actamat.2008.11.042.

[102] M. Hernández-Mayoral, D. Gómez-Briceño, Transmission electron microscopy study on neutron irradiated pure iron and RPV model alloys, J. Nucl. Mater. 399 (2–3) (2010) 146–153, https://doi.org/10.1016/j.jnucmat.2009.11.013.

[103] K. Arakawa, M. Hatanaka, E. Kuramoto, K. Ono, H. Mori, Changes in the Burgers Vector of Perfect Dislocation Loops without Contact with the External Dislocations, Phys. Rev. Lett. 96 (2006), 125506, https://doi.org/10.1103/PhysRevLett.96.125506.

[104] K. Arakawa, K. Ono, M. Isshiki, K. Mimura, M. Uchikoshi, H. Mori, Observation of the One-Dimensional Diffusion of Nanometer-Sized Dislocation Loops, Science 318 (5852) (2007) 956–959, https://doi.org/10.1126/science.1145386.

[105] Z. Yao, M.L. Jenkins, M. Hernández-Mayoral, M.A. Kirk, The temperature dependence of heavy-ion damage in iron: a microstructural transition at elevated temperatures, Philos. Mag. A 90 (35-36) (2010) 4623–4634, https://doi.org/10.1080/14786430903430981.

[106] Y. Zhang, X.-M. Bai, M.R. Tonks, S.B. Biner, Formation of prismatic loops from C15 Laves phase interstitial clusters in body-centered cubic iron, Scr. Mater. 98 (2015) 5–8, https://doi.org/10.1016/j.scriptamat.2014.10.033.

[107] A. Chartier, M.-C. Marinica, Rearrangement of interstitial defects in alpha-Fe under extreme condition. Acta Materialia, 2019, 180, 141-148.

[108] J. Marian, B.D. Wirth, J.M. Perlado, Mechanism of Formation and Growth of ⟨100⟩ Interstitial Loops in Ferritic Materials. Phys. Rev. Lett. 88, 255507. 2002. DOI: 10.1103/PhysRevLett.88.255507.

[109] C. Domain, C.S. Becquart, Solute – <111> interstitial loop interaction in α-Fe: A DFT study, J. Nucl. Mater. 499 (2018) 582–594, https://doi.org/10.1016/j.jnucmat.2017.10.070.

[110] H. Mehrer, Diffusion in Solids : Fundamentals, Methods, Materials, Diffusion controlled processes, Springer-Verlag, Berlin, 2007.

[111] Y.N. Osetsky, Atomistic Study of Diffusional Mass Transport in Metals, Defect and Diffusion Forum 188–190 (2001) 71–92, https://doi.org/10.4028/www.scientific.net/ddf.188-190.71.

[112] M. Wen, N.M. Ghoniem, B.N. Singh, Dislocation decoration and raft formation in irradiated materials, Phil. Mag. 85 (22) (2005) 2561–2580, https://doi.org/10.1080/14786430500154281.

[113] T.S. Hudson, S.L. Dudarev, M.-J. Caturla, A.P. Sutton, Effects of elastic interactions on post-cascade radiation damage evolution in kinetic Monte Carlo simulations, Phil. Mag. 85 (4–7) (2006) 661–675, https://doi.org/10.1080/14786430412331320026.

[114] M. Wen, A. Takahashi, N.M. Ghoniem, Kinetics of self-interstitial cluster aggregation near dislocations and their influence on hardening, J. Nucl. Mater. 392 (3) (2009) 386–395, https://doi.org/10.1016/j.jnucmat.2008.10.029.

[115] A.B. Sivak, V.M. Chernov, V.A. Romanov, P.A. Sivak, Kinetic Monte-Carlo simulation of self-point defect diffusion in dislocation elastic fields in bcc iron and vanadium, J. Nucl. Mater. 417 (1–3) (2011) 1067–1070, https://doi.org/10.1016/j.jnucmat.2010.12.176.

[116] D. Carpentier, T. Jourdan, Y. Le Bouar, M.-C. Marinica, Effect of saddle point anisotropy of point defects on their absorption by dislocations and cavities, Acta Mater. 136 (2017) 323–334, https://doi.org/10.1016/j.actamat.2017.07.013.

[117] T. Jourdan, A. Vattré, A continuous model including elastodiffusion for sink strength calculation of interfaces, Comput. Mater. Sci. 153 (2018) 473–478, https://doi.org/10.1016/j.commatsci.2018.07.023.

[118] A. Vattré, T. Jourdan, H. Ding, M.-C. Marinica, M.J. Demkowicz, Non-random walk diffusion enhances the sink strength of semicoherent interfaces, Nat. Commun. 7 (2016) 10424, https://doi.org/10.1038/ncomms10424.

[119] N. Anento, L. Malerba, A. Serra, Edge dislocations as sinks for sub-nanometric radiation induced defects in α-iron, J. Nucl. Mater. 498 (2018) 341–347, https://doi.org/10.1016/j.jnucmat.2017.10.053.

[120] H.A. Khater, G. Monnet, D. Terentyev, A. Serra, Dislocation glide in Fe–carbon solid solution: from atomic to continuum level description, Int. J. Plast. 62 (2014) 34–49, https://doi.org/10.1016/j.ijplas.2014.06.006.

[121] Osetsky Y.N. Rodney D. Atomic-Level Dislocation Dynamics in Irradiated Metals," in R. Koningsand, R.E. Stoller (eds.) Comprehensive Nuclear Materials 2nd ed., 2020, (Oxford: Elsevier.) 1, 663–688.

[122] S.L. Dudarev, A.P. Sutton, Elastic interactions between nano-scale defects in irradiated materials, Acta Mater. 125 (2017) 425–430, https://doi.org/10.1016/j.actamat.2016.11.060.

[123] S.L. Dudarev, D.R. Mason, E. Tarleton, P.-W. Ma, A.E. Sand, A multi-scale model for stresses, strains and swelling of reactor components under irradiation, Nucl. Fusion 58 (12) (2018) 126002, https://doi.org/10.1088/1741-4326/aadb48.

[124] J.S. Wróbel, M.R. Zemła, D. Nguyen-Manh, P. Olsson, L. Messina, C. Domain, T. Wejrzanowski, S.L. Dudarev, Elastic dipole tensors and relaxation volumes of point defects in concentrated random magnetic Fe-Cr alloys. arXiv:2007.15424v1 [cond-mat.mtrl-sci]. 2020, Available at: https://arxiv.org/abs/2007.15424 (Accessed January 3rd, 2021).

[125] V. Jansson, L. Malerba, A. De Backer, C.S. Becquart, C. Domain, Sink strength calculations of dislocations and loops using OKMC, J. Nucl. Mater. 442 (1–3) (2013) 218–226, https://doi.org/10.1016/j.jnucmat.2013.08.052.

[126] Z. Rong, Y.N. Osetsky, D.J. Bacon, A model for the dynamics of loop drag by a gliding dislocation, Phil. Mag. 85 (14) (2005) 1473–1493, https://doi.org/10.1080/14786430500036371.

[127] K.G. Field, S.A. Briggs, X. Hu, Y. Yamamoto, R.H. Howard, K. Sridharan, Heterogeneous dislocation loop formation near grain boundaries in a neutron-irradiated commercial FeCrAl alloy. J. Nucl. Mater. 483, 2017 54-61 Doi: 0.1016/j.jnucmat.2016.10.050.

[128] X.-M. Bai, A.F. Voter, R.G. Hoagland, M. Nastasi, B.P. Uberuaga, Efficient Annealing of Radiation Damage Near Grain Boundaries via Interstitial Emission, Science 327 (5973) (2010) 1631–1634, https://doi.org/10.1126/science.1183723.

[129] D.R. Mason, A.E. Sand, S.L. Dudarev, Atomistic-Object Kinetic Monte Carlo simulations of irradiation damage in tungsten. arXiv:1904.04089 [cond-mat.mtrl-sci]. 2019, DOI: 10.1088/1361-651X/ab1a1e.

[130] L. Malerba, C.S. Becquart, C. Domain, Object kinetic Monte Carlo study of sink strengths, J. Nucl. Mater. 360 (2007) 159–169, https://doi.org/10.1016/j.jnucmat.2006.10.002 (and references therein).

[131] H. Wiedersich, On the theory of void formation during irradiation, Radiation Effects 12 (1-2) (1972) 111–125, https://doi.org/10.1080/00337577208231128.

[132] F. Nichols, On the estimation of sink-absorption terms in reaction-rate-theory analysis of radiation damage, J. Nucl. Mater. 75 (1) (1978) 32–41, https://doi.org/10.1016/0022-3115(78)90026-0.

[133] A.D. Brailsford, J.R. Matthews, R. Bullough, The effect of recombination on sink strengths in the rate theory of void-swelling, J. Nucl. Mater. 79 (1) (1979) 1–13, https://doi.org/10.1016/0022-3115(79)90428-8.

[134] R. Bullough, M.R. Hayns, M.H. Wood, Sink strengths for thin film surfaces and grain boundaries, J. Nucl. Mater. 90 (1–3) (1980) 44–59, https://doi.org/10.1016/0022-3115(80)90244-5.

[135] A.D. Brailsford, R. Bullough, The theory of sink strengths, Philosoph. Trans. Roy. Soc. London. Series A, Mathemat. Phys. Sci. 302 (1465) (1981) 87–137, https://doi.org/10.1098/rsta.1981.0158.

[136] A.V. Barashev, S.I. Golubov, H. Trinkaus, Reaction kinetics of glissile interstitial clusters in a crystal containing voids and dislocations, Philos. Mag. A 81 (10) (2001) 2515–2532, https://doi.org/10.1080/01418610108217161.

[137] H. Trinkaus, H.L. Heinisch, A.V. Barashev, S.I. Golubov, B.N. Singh, 1D to 3D diffusion-reaction kinetics of defects in crystals, Physical Review B 66 (2002) 060105(R), https://doi.org/10.1103/PhysRevB.66.060105.

[138] B.N. Singh, N.M. Ghoniem, H. Trinkaus, Experiment-based modelling of hardening and localized plasticity in metals irradiated under cascade damage conditions, J. Nucl. Mater. 307–311 (2002) 159–170, https://doi.org/10.1016/S0022-3115(02)01095-4.

[139] A. Bakaev, D. Terentyev, Z. Chang, M. Posselt, P. Olsson, E.E. Zhurkin, Effect of isotropic stress on dislocation bias factor in bcc iron: an atomistic study, Phil. Mag. 98 (1) (2018) 54–74, https://doi.org/10.1080/14786435.2017.1390325.

[140] J. Boisse, A. De Backer, C. Domain, C. Becquart, Modeling of the self-trapping of helium and the trap mutation in tungsten using DFT and empirical potentials based on DFT, J. Mater. Res. 29 (20) (2014) 2374–2386, https://doi.org/10.1557/jmr.2014.258.

[141] L.J. Cuddy, Recovery of point defects in iron after low-temperature deformation, Acta Metall. 16 (1) (1968) 23–28, https://doi.org/10.1016/0001-6160(68)90067-9.

[142] A. Vehanen, P. Hautojärvi, J. Johansson, J. Yli-Kauppila, P. Moser, Vacancies and carbon impurities in α- iron: Electron irradiation, Physical Review B 25 (1982) 762, https://doi.org/10.1103/PhysRevB.25.762.

[143] T. Tabata, H. Fujita, H. Ishii, K. Igaki, M. Isshiki, Determination of mobility of lattice vacancies in pure iron by high voltage electron microscopy, Scr. Metall. 15 (12) (1981) 1317–1321, https://doi.org/10.1016/0036-9748(81)90090-9.

[144] T. Jourdan, G. Stoltz, F. Legoll, L. Monasse, An accurate scheme to solve cluster dynamics equations using a Fokker-Planck approach, Comput. Phys. Commun. 207 (2016) 170–178, https://doi.org/10.1016/j.cpc.2016.06.001.

[145] P. Terrier, M. Athènes, T. Jourdan, G. Adjanor, G. Stoltz, Cluster dynamics modelling of materials: A new hybrid deterministic/stochastic coupling approach, J. Comput. Phys. 350 (2017) 280–295, https://doi.org/10.1016/j.jcp.2017.08.015.

[146] M.I. Mendelev, S. Han, D.J. Srolovitz, G.J. Ackland, D.Y. Sun, M. Asta, Development of new interatomic potentials appropriate for crystalline and liquid

[147] E. Vincent, Simulation numérique à l'échelle atomique de l'évolution microstructurale sous irradiation d'alliages ferritiques. PhD dissertation, University of Lille, Lille, France, 2006.

[148] L. Messina, Multiscale modeling of atomic transport phenomena in ferritic steels, PhD dissertation, Royal Technical University (KTH), Stockholm, Sweden, 2015.

[149] S.I. Golubov, B.N. Singh, H. Trinkaus, Defect accumulation in fcc and bcc metals and alloys under cascade damage conditions: Towards a generalisation of the production bias model, J. Nucl. Mater. 276 (1-3) (2000) 78–89, https://doi.org/10.1016/S0022-3115(99)00171-3.

[150] H. Trinkaus, B.N. Singh, S.I. Golubov, Progress in modelling the microstructural evolution in metals under cascade damage conditions, J. Nucl. Mater. 283–287 (Part 1) (2000) 89–98, https://doi.org/10.1016/S0022-3115(00)00332-9.

[151] J. Marian, B.D. Wirth, R. Schäublin, G.R. Odette, J.M. Perlado, MD modeling of defects in Fe and their interactions, J. Nucl. Mater. 323 (2-3) (2003) 181–191, https://doi.org/10.1016/j.jnucmat.2003.08.037.

[152] D. Terentyev, N. Anento, A. Serra, V. Jansson, H. Khater, G. Bonny, Interaction of carbon with vacancy and self-interstitial atom clusters in α-iron studied using metallic–covalent interatomic potential, J. Nucl. Mater. 408 (3) (2011) 272–284, https://doi.org/10.1016/j.jnucmat.2010.11.053.

[153] D. Terentyev, N. Anento, A. Serra, Interaction of <100> loops with Carbon atoms and <100> dislocations in BCC Fe: An atomistic study, J. Nucl. Mater. 420 (2012) 9–15, https://doi.org/10.1016/j.jnucmat.2011.08.037.

[154] N. Anento, A. Serra, Carbon–vacancy complexes as traps for self-interstitial clusters in Fe–C alloys, J. Nucl. Mater. 440 (1-3) (2013) 236–242, https://doi.org/10.1016/j.jnucmat.2013.04.087.

[155] R. Candela, N. Mousseau, R.G.A. Veiga, C. Domain, C.S. Becquart, Interaction between interstitial carbon atoms and a ½⟨1 1 1⟩ self-interstitial atoms loop in an iron matrix: a combined DFT, off lattice KMC and MD study, J. Phys.: Condens. Matter 30 (33) (2018) 335901, https://doi.org/10.1088/1361-648X/aad25d.

[156] C.J. Först, J. Slycke, K.J. Van Vliet, S. Yip, Point Defect Concentrations in Metastable Fe-C Alloys, Phys. Rev. Lett. 96 (2006), 175501, https://doi.org/10.1103/PhysRevLett.96.175501.

[157] C.-C. Fu, E. Meslin, A. Barbu, F. Willaime, V. Oison, Effect of C on Vacancy Migration in α-Iron Solid State Phenomena, 139, 2008 pp. 157-164 DOI. 10.4028/www.scientific.net/ssp.139.157.

[158] C. Barouh, T. Schuler, C.-C. Fu, M. Nastar, Interaction between vacancies and interstitial solutes (C, N, and O) in α−Fe: From electronic structure to thermodynamics, Physical Review B 90 (2014), 054112, https://doi.org/10.1103/PhysRevB.90.054112.

[159] C. Barouh, T. Schuler, C.-C. Fu, T. Jourdan, Predicting vacancy-mediated diffusion of interstitial solutes in α-Fe, Physical Review B 92 (2015), 104102, https://doi.org/10.1103/PhysRevB.92.104102.

[160] M.J. Konstantinovic, L. Malerba, Dissolution of carbon-vacancy complexes in Fe-C alloys, Physical Review Materials 1 (2017), 053602, https://doi.org/10.1103/PhysRevMaterials.1.053602.

[161] C. Domain, C.S. Becquart, Ab initio calculations of defects in Fe and dilute Fe-Cu alloys, Physical Review B 65 (2001), 024103, https://doi.org/10.1103/PhysRevB.65.024103.

[162] M. Ludwig, D. Farkas, D. Pedraza, S. Schmauder, Embedded atom potential for Fe-Cu interactions and simulations of precipitate-matrix interfaces. Model. Simulat. Mater. Sci. Eng. 6, 19-. 1998, DOI: 10.1088/0965-0393/6/1/003.

[163] G.J. Ackland, D.J. Bacon, A.F. Calder, T. Harry, Computer simulation of point defect properties in dilute Fe—Cu alloy using a many-body interatomic potential, Philos. Mag. A 75 (3) (1997) 713–732, https://doi.org/10.1080/01418619708207198.

[164] J.R. Beeler, R.A. Johnson, Vacancy Clusters in α-Iron, Phys. Rev. 156 (3) (1967) 677–684, https://doi.org/10.1103/PhysRev.156.677.

[165] A. Hardouin Duparc, C. Moingeon, N. Smetniansky-de-Grande, A. Barbu, Microstructure modelling of ferritic alloys under high flux 1 MeV electron irradiations, J. Nucl. Mater. 302 (2-3) (2002) 143–155, https://doi.org/10.1016/S0022-3115(02)00776-6.

[166] A. Seeger, Lattice Vacancies in High-Purity α-Iron, Physica status solidi (a) 167 (2) (1998) 289–311, https://doi.org/10.1002/(SICI)1521-396X(199806)167:2<289::AID-PSSA289>3.0.CO;2-V.

[167] G. Lucas, R. Schäublin, Vibrational contributions to the stability of point defects in bcc iron: A first-principles study, Nucl. Instrum. Methods Phys. Res., Sect. B 267 (18) (2009) 3009–3012, https://doi.org/10.1016/j.nimb.2009.06.110.

[168] L. Messina, M. Nastar, N. Sandberg, P. Olsson, Systematic electronic-structure investigation of substitutional impurity diffusion and flux coupling in bcc iron, Physical Review B 93 (2016), 184302, https://doi.org/10.1103/PhysRevB.93.184302.

[169] L. Messina, T. Schuler, M. Nastar, M.-C. Marinica, P. Olsson, Solute diffusion by self-interstitial defects and radiation-induced segregation in ferritic Fe-X (X=Cr, Cu, Mn, Ni, P, Si) dilute alloys, Acta Mater. 191 (2020) 166–185, https://doi.org/10.1016/j.actamat.2020.03.038.

[170] S.I. Golubov, R.E. Stoller, S.J. Zinkle, A.M. Ovcharenko, Kinetics of coarsening of helium bubbles during implantation and post-implantation annealing, J. Nucl.

Mater. 361 (2–3) (2007) 149–159, https://doi.org/10.1016/j.jnucmat.2006.12.032.

[171] M. Biget, R. Rizk, P. Vajda, A. Bessis, On the spontaneous recombination volume of Frenkel defects in irradiated b.c.c. metals, Solid State Commun. 16 (7) (1975) 949–952, https://doi.org/10.1016/0038-1098(75)90901-1.

[172] J. Dural, J. Ardonceau, J.C. Roussett, Endommagement du fer par irradiation aux électrons à 20 K, Le J. Physique France 38 (8) (1977) 1007–1011, https://doi.org/10.1051/jphys:019770038080100700.

[173] R.E. Stoller, "Modelling the influence of irradiation temperature and displacement rate pn hardening due to point-defect clusters in ferritic steels," in Effects of Radiation on Materials: 16th International Symposium, ASTM STP 1175, ed. A.S. Kumar, D.S. Gelles, R.K. Nanstad and E.A. Little (ASTM, Philadelphia), 1993, 394-422.

[174] A. Souidi, M. Hou, C.S. Becquart, C. Domain, Atomic displacement cascade distributions in iron, J. Nucl. Mater. 295 (2-3) (2001) 179–188, https://doi.org/10.1016/S0022-3115(01)00556-6.

[175] K. Nakashima, R.E. Stoller, H. Xu, Recombination radius of a Frenkel pair and capture radius of a self-interstitial atom by vacancy clusters in bcc Fe, J. Phys.: Condens. Matter 27 (33) (2015) 335401, https://doi.org/10.1088/0953-8984/27/33/335401.

[176] M.A. Puigví, Y.N. Osetsky, A. Serra, Point-defect clusters and dislocation loops in bcc metals: continuum and atomistic study, Phil. Mag. 83 (7) (2003) 857–871, https://doi.org/10.1080/0141861021000055682.

[177] D. Terentyev, L. Malerba, Interaction of <100> and ½<111> dislocation loops with point defects in ferritic alloys, J. Nucl. Mater. 377 (1) (2008) 141–146, https://doi.org/10.1016/j.jnucmat.2008.02.062.

[178] G.J. Ackland, M.I. Mendelev, D.J. Srolovitz, S. Han, A.V. Barashev, Development of an interatomic potential for phosphorus impurities in α-iron, J. Phys.: Condens. Matter 16 (27) (2004) S2629, https://doi.org/10.1088/0953-8984/16/27/003.

[179] M.A. Puigví, Y.N. Osetsky, A. Serra, Interactions between vacancy and glissile interstitial clusters in iron and copper, Mater. Sci. Eng., A 365 (1) (2004) 101–106, https://doi.org/10.1016/j.msea.2003.09.013.

[180] D. Terentyev, Study of Radiation Effects in FeCr Alloys for Fusion Applications Using Computer Simulations. PhD dissertation, Université Libre de Bruxelles, Brussels, Belgium, 2006.

[181] N. Anento, A. Serra, Interaction of a mobile {112} grain boundary with radiation induced defects in α-Fe: Transformation of defects and impact on the shear-coupled grain boundary migration. Computat. Mater. Sci. 179, 109679. DOI. 10.1016/j.commatsci.2020.109679.

[182] L. Messina, M. Nastar, T. Garnier, C. Domain, P. Olsson, Exact ab initio transport coefficients in bcc Fe-X (X=Cr, Cu, Mn, Ni, P, Si) dilute alloys, Physical Review B 90 (2014), 104203, https://doi.org/10.1103/PhysRevB.90.104203.

[183] C.J. Ortiz, P. Pichler, T. Fühner, F. Cristiano, B. Colombeau, N.E.B. Cowern, A. Claverie, A physically based model for the spatial and temporal evolution of self-interstitial agglomerates in ion-implanted silicon, J. Appl. Phys. 96 (9) (2004) 4866–4877, https://doi.org/10.1063/1.1786678.